Title

A kinetochore-associated kinesin-7 motor cooperates with BUB3.3 to regulate mitotic chromosome congression in Arabidopsis thaliana

Authors

Tang, Xiaoya

He, Ying

Tang, Yihang

et al.

Publication Date

2024-10-16

DOI

10.1038/s41477-024-01824-7

nature plants

Article

https://doi.org/10.1038/s41477-024-01824-7

A kinetochore-associated kinesin-7 motor cooperates with BUB3.3 to regulate mitotic chromosome congression in *Arabidopsis thaliana*

Received: 6 April 2024

Accepted: 20 September 2024

Published online: 16 October 2024

Check for updates

Xiaoya Tang[1], Ying He[1], Yihang Tang[1], Keqi Chen[1], Honghui Lin[1], Bo Liu[2] & Xingguang Deng[1]

Faithful genome partition during cell division relies on proper congression of chromosomes to the spindle equator before sister chromatid segregation. Here we uncover a kinesin-7 motor, kinetochore-associated kinesin 1 (KAK1), that is required for mitotic chromosome congression in *Arabidopsis*. KAK1 associates dynamically with kinetochores throughout mitosis. Loss of KAK1 results in severe defects in chromosome congression at metaphase, yet segregation errors at anaphase are rarely observed. KAK1 specifically interacts with the spindle assembly checkpoint protein BUB3.3 and both proteins show interdependent kinetochore localization. Chromosome misalignment in BUB3.3-depleted plants can be rescued by artificial tethering of KAK1 to kinetochores but not vice versa, demonstrating that KAK1 acts downstream of BUB3.3 to orchestrate microtubule-based chromosome transport at kinetochores. Moreover, we show that KAK1's motor activity is essential for driving chromosome congression to the metaphase plate. Thus, our findings reveal that plants have repurposed BUB3.3 to interface with a specialized kinesin adapted to integrate proper chromosome congression and checkpoint control through a distinct kinetochore design.

The equal segregation of duplicated chromosomes to daughter cells is fundamental to organism development and reproduction. This complex process requires proper amphitelic attachment of sister kinetochores to microtubules from opposite spindle poles. To achieve bipolar attachment, chromosomes must congress from dispersed positions in the cell to align precisely at the metaphase plate. Chromosome congression facilitates the directed migration of polar chromosomes to the spindle equator, enabling kinetochore pairs on each chromosome to become oriented in the same plane[1]. Without congression, polar chromosomes fail to migrate to the metaphase plate, resulting in aberrant kinetochore–microtubule attachments and catastrophic chromosome missegregation[2]. To prevent such segregation defects, eukaryotic cells have evolved the spindle assembly checkpoint (SAC) as a surveillance mechanism to delay anaphase until all chromosomes achieve bipolar attachment[3]. SAC signalling from unattached kinetochores inhibits the anaphase-promoting complex/cyclosome to delay sister chromatid separation[3–5]. Aberrations in these intricate mechanisms lead to aneuploidy and multiple developmental syndromes.

The kinesin-7 family motor, centromere protein E (CENP-E), plays a central role in chromosome congression and alignment during cell division in many eukaryotes[6,7]. In animal cells, CENP-E localizes to the fibrous corona of the outer kinetochore and remains enriched

[1]Key Laboratory of Bio-Resource and Eco-Environment of Ministry of Education, College of Life Sciences, Sichuan University, Chengdu, China. [2]Department of Plant Biology, College of Biological Sciences, University of California, Davis, CA, USA. e-mail: xgdeng@scu.edu.cn

at kinetochores during mitosis[8]. The C-terminal region of CENP-E mediates its targeting to kinetochores, and this region has been found to directly bind to the SAC protein budding uninhibited by benzimidazoles-related 1 (BUBR1)[9–11]. Upon activation of the SAC, CENP-E is rapidly recruited to kinetochores within minutes in a BUBR1-dependent manner that is essential for proper chromosome alignment[12]. Once localized at kinetochores, CENP-E utilizes its plus-end directed microtubule motility to transport mono-oriented chromosomes to the spindle equator[13–15]. When CENP-E is inhibited or depleted, chromosomes remain scattered near the spindle poles instead of aligning at the metaphase plate[8]. It is believed that the interaction between CENP-E and BUBR1 couples the SAC signalling pathway with CENP-E-dependent transport of chromosomes to the metaphase plate[16,17]. This coordination ensures that chromosomes are properly aligned before the onset of anaphase, thereby preserving genomic integrity during cell division.

Despite the well-established importance of CENP-E and SAC in regulating chromosome congression and error correction during cell division, these pathways remain poorly explored in plants. The *Arabidopsis thaliana* genome encodes a large family of 15 kinesin-7 isoforms[18–20], which are the plant homologues of the animal CENP-E kinesin. However, it remains unclear whether one or more of these plant-specific kinesins play functional roles analogous to CENP-E in mediating chromosome congression, and whether they are integrated with the SAC signalling pathways. Our recent work has revealed a distinct functional mode for the non-canonical budding uninhibited by benzimidazoles 3 (BUB3) family protein BUB3.3 in *Arabidopsis*, demonstrating that it facilitates SAC activation but does not recruit other SAC components in the same manner as observed in other organisms[21]. Interestingly, loss of BUB3.3 leads to frequent misalignment of chromosomes during mitosis and this chromosome miscongression phenotype was not observed in other SAC mutants[21]. This suggests that BUB3.3 may have SAC-independent functions in regulating chromosome movement; however, its molecular interactions and underlying mechanisms mediating this process remain unknown in plants.

Chromosome congression defects resulting from the loss of BUB3.3 in *Arabidopsis* are reminiscent of the phenotypes observed upon depletion of the CENP-E kinesin in animals. This observation raises the intriguing possibility that BUB3.3 may cooperate with an unidentified CENP-E-like motor protein to regulate chromosome congression in plants. To identify potential kinetochore-associated partners of BUB3.3 that could be involved in this process, we immunopurified BUB3.3 from *Arabidopsis* and uncovered a previously unreported member of the kinesin-7 family. We demonstrate that this kinesin motor exhibits dynamic localization to kinetochores dependent on BUB3.3 and is essential for proper chromosome alignment at the metaphase plate. Our results reveal a kinetochore-associated kinesin-7 motor in plants that cooperates with BUB3.3 to regulate chromosome movements and ensure the fidelity of cell division processes.

Results

KAK1 associates with kinetochores throughout mitosis

Our immunoprecipitation–mass spectrometry (MS) experiments using green fluorescent protein (GFP)–BUB3.3 as bait identified a kinesin motor protein encoded by the *At3g10180* locus as a top interacting partner (Supplementary Data 1, see the detailed interaction results provided below). This finding is consistent with a previous study that also reported the At3g10180 protein as being BUB3.3 associated[22]. Phylogenetic analysis revealed that this gene encodes an unstudied member of the kinesin-7 family in *A. thaliana*[23], and the protein shares a close evolutionary relationship with the animal CENP-E protein (Extended Data Fig. 1). However, sequence alignment showed that this plant kinesin-7 protein displays poor overall sequence conservation compared with CENP-E, with the primary region of sequence similarity being confined to the motor domain (Supplementary Fig. 1). Because of its physical association with kinetochores and the mitotic roles uncovered here, we named this kinesin kinetochore-associated kinesin 1 (KAK1).

We first isolated a homozygous transfer DNA insertional mutant of KAK1 with the insertion in the 25th exon (*kak1*; Fig. 1a and Supplementary Fig. 2). The *kak1* mutant grew indistinguishably from the wild-type (WT) plants under normal conditions. However, *kak1* seedlings exhibited notable growth retardation when challenged with 100 nM microtubule-depolymerizing drug oryzalin, as quantified by shorter root lengths compared with WT (Fig. 1b,c). This oryzalin hypersensitivity phenotype was fully suppressed when a KAK1–GFP fusion was expressed under the native *KAK1* promoter in *kak1* plants (Fig. 1b,c). These results indicate the oryzalin sensitivity is caused by loss of *KAK1* and the KAK1–GFP fusion is functional.

The functionality of KAK1–GFP allowed us to examine KAK1 subcellular localization during mitosis using immunofluorescence microscopy. At prophase, concentrated KAK1–GFP signal was detected on the nuclear envelope before nuclear envelope breakdown (NEB) (Fig. 1d). After NEB at prometaphase, KAK1–GFP appeared as paired dots associated with chromosomes within the bipolar spindle (Fig. 1d). At metaphase when chromosomes were aligned at the equatorial plate, KAK1–GFP signals were present at the two edges of aligned chromosomes and the end of kinetochore fibres (Fig. 1d). As chromosomes segregated at anaphase, dot-like KAK1–GFP signals tracked along shortening kinetochore microtubules moving towards the poles until they reached the two spindle poles at telophase (Fig. 1d). During cytokinesis when the phragmoplast formed, the KAK1–GFP signal diffused from the kinetochores into the cytoplasm (Fig. 1d). This dynamic localization pattern indicates KAK1 associates with kinetochores throughout mitosis after NEB and before reformation of daughter nuclei.

Loss of KAK1 causes chromosome congression errors

The observed localization of KAK1 to kinetochores prompted us to test whether its loss led to errors in mitosis. Although the *kak1* mutant appeared phenotypically normal, closer examination revealed specific defects in chromosome alignment during mitosis. In WT metaphase cells, chromosomes achieved complete congression and aligned precisely at the cell equator between separated kinetochore fibre arrays (Extended Data Fig. 2a). By contrast, *kak1* mutant cells frequently exhibited misaligned 'polar' chromosomes positioned near the spindle poles despite forming a bipolar spindle (Extended Data Fig. 2a). Quantification of these mitotic defects revealed a notable increase in the percentage of *kak1* mutant cells (67.4%, $n = 135$) displaying misaligned chromosomes at metaphase, compared with the WT cells (0%, $n = 105$) (Extended Data Fig. 2b). Furthermore, oryzalin treatment could further exacerbate the chromosome congression defects in the *kak1* mutant, with a higher proportion of the mutant cells (89.4%, $n = 113$) exhibiting misaligned chromosomes (Extended Data Fig. 2b).

To monitor mitotic progression in vivo, we delivered a histone H1.2–red fluorescent protein (RFP) marker labelling chromosomes as well as a GFP–TUB6 marker labelling microtubules into *kak1* and WT plants. In WT cells, following bipolar spindle assembly after NEB, chromosomes congressed synchronously from initially scattered positions throughout the cell, becoming stably bioriented at the spindle equator before anaphase onset within 10 min. Sister chromatids then separated smoothly during anaphase and segregated into two daughter nuclei on either side of the expanding phragmoplast (100% of 18 cells) (Fig. 2a and Supplementary Video 1). In *kak1* mitotic cells, the majority of chromosomes congressed normally to the metaphase plate. However, a subset of chromosomes frequently detached and migrated from the metaphase plate back towards the spindle poles. Despite the prominent polar chromosomes in *kak1* cells, anaphase onset was delayed (more than 30 min) until the misaligned chromosomes re-established metaphase plate alignment (61.9% of 21 cells) (Fig. 2b and Supplementary Video 2). These results suggest that although chromosome congression defects occur more often in *kak1* mutant cells, the SAC remains active

https://doi.org/10.1038/s41477-024-01824-7

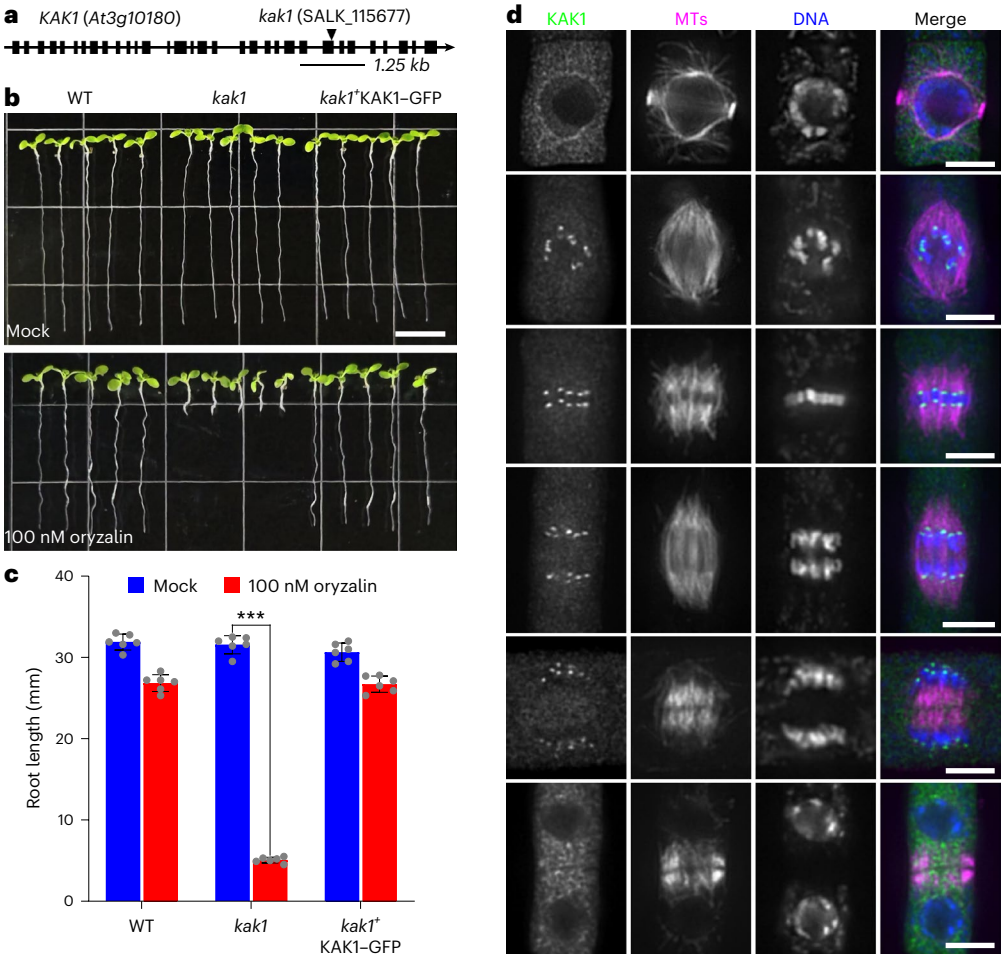

Fig. 1 | KAK1 associates with kinetochores throughout mitotic cell division. **a**, Gene structure and transfer DNA insertion of *KAK1* (*At3g10180*). Exons are represented by black boxes and introns by lines. **b**, Seedling of the WT, *kak1* mutant and *kak1* mutant expressing *pKAK1*::KAK1–GFP with and without 100 nM oryzalin treatment at 10 days. Scale bars, 1 cm. **c**, Quantification of root lengths in the seedlings with and without oryzalin treatment. Bars represent means ± s.d. of six seedlings per genotype. The statistical significance (***$P < 10^{-6}$) was determined by one-way ANOVA with post-hoc Tukey's test. The experiment was repeated three times with similar results. **d**, Triple localization of KAK1, microtubules (MTs) and DNA by immunofluorescence throughout the cell cycle, the merged images have KAK1–GFP detected by the anti-GFP antibody in green, microtubules detected by the anti-tubulin antibody in magenta, and DNA detected by DAPI in blue. Micrographs are representative of more than 100 cells from three independent lines with similar results. Scale bars, 5 µm.

and inhibits sister chromatid separation until all chromosomes are bioriented properly.

KAK1 interacts directly with BUB3.3

Proteomic screening experiments identified KAK1 as a BUB3.3-assembled protein, and the chromosome misalignment phenotype of *kak1* mutant cells resembles *bub3.3* mutant cells. This prompted us to explore the potential relationship between the two proteins. To validate whether KAK1 and BUB3.3 associated with each other in vivo, we performed reciprocal co-immunoprecipitation experiments using KAK1–GFP and GFP–BUB3.3 rescue plants. GFP–BUB3.3 immunoprecipitation identified 85 unique KAK1 peptides by MS, covering 60.7% of the KAK1 sequence. Conversely, the KAK1–GFP immunoprecipitation preparations recovered BUB3.3, with 15 unique peptides representing 52.2% sequence coverage. By contrast, neither KAK1 nor BUB3.3 was detected when GFP alone was used as a negative control bait (Fig. 3a and Supplementary Data 1 and 2). We next examined whether KAK1 and BUB3.3 co-localize during mitosis by expressing KAK1–FLAG in *bub3.3* plants complemented with functional GFP–BUB3.3. Immunofluorescence microscopy revealed that KAK1–FLAG co-localized precisely with GFP–BUB3.3 at kinetochores from prophase through anaphase (Fig. 3b). Thus, we conclude that KAK1 and BUB3.3 specifically associate with each other at kinetochores in planta.

We further used a yeast two-hybrid (Y2H) assay to test whether KAK1 interacted directly with BUB3.3 (Fig. 3c). To screen which region of KAK1 mediates BUB3.3 binding, we made multiple KAK1 deletion constructs based on domain prediction analysis using the SMART tool (http://smart.embl-heidelberg.de). According to SMART analysis, the KAK1 protein consists of an N-terminal motor head, a C-terminal tail and an intervening stalk region harbouring two internal repeats (IRs) flanked by coiled coils (Fig. 3c). Interestingly, amino acid sequence similarity between the two IR domains within the KAK1 stalk region is relatively low (Supplementary Fig. 3). We then created a series of KAK1 truncation constructs expressing the motor, tail or stalk region with IRs, in addition to the full-length KAK1 protein. A Y2H assay revealed that the KAK1 motor and tail regions failed to interact with BUB3.3. However, the N-terminal half of KAK1, encompassing residues 1–600, was sufficient to bind BUB3.3, similar to the full-length protein. Further mapping showed that amino acids between residues 434 and 600 of KAK1, which includes the first IR (IR1) motif, are required for the interaction with BUB3.3. Deleting this IR1 domain within KAK1 abolished the binding to BUB3.3 (Fig. 3c). The physical interaction between BUB3.3 and KAK1 was further confirmed using an in vitro pull-down assay. Recombinant GST–BUB3.3 purified from *Escherichia coli* was able to pull down bacterially expressed maltose binding protein (MBP)-fused

https://doi.org/10.1038/s41477-024-01824-7

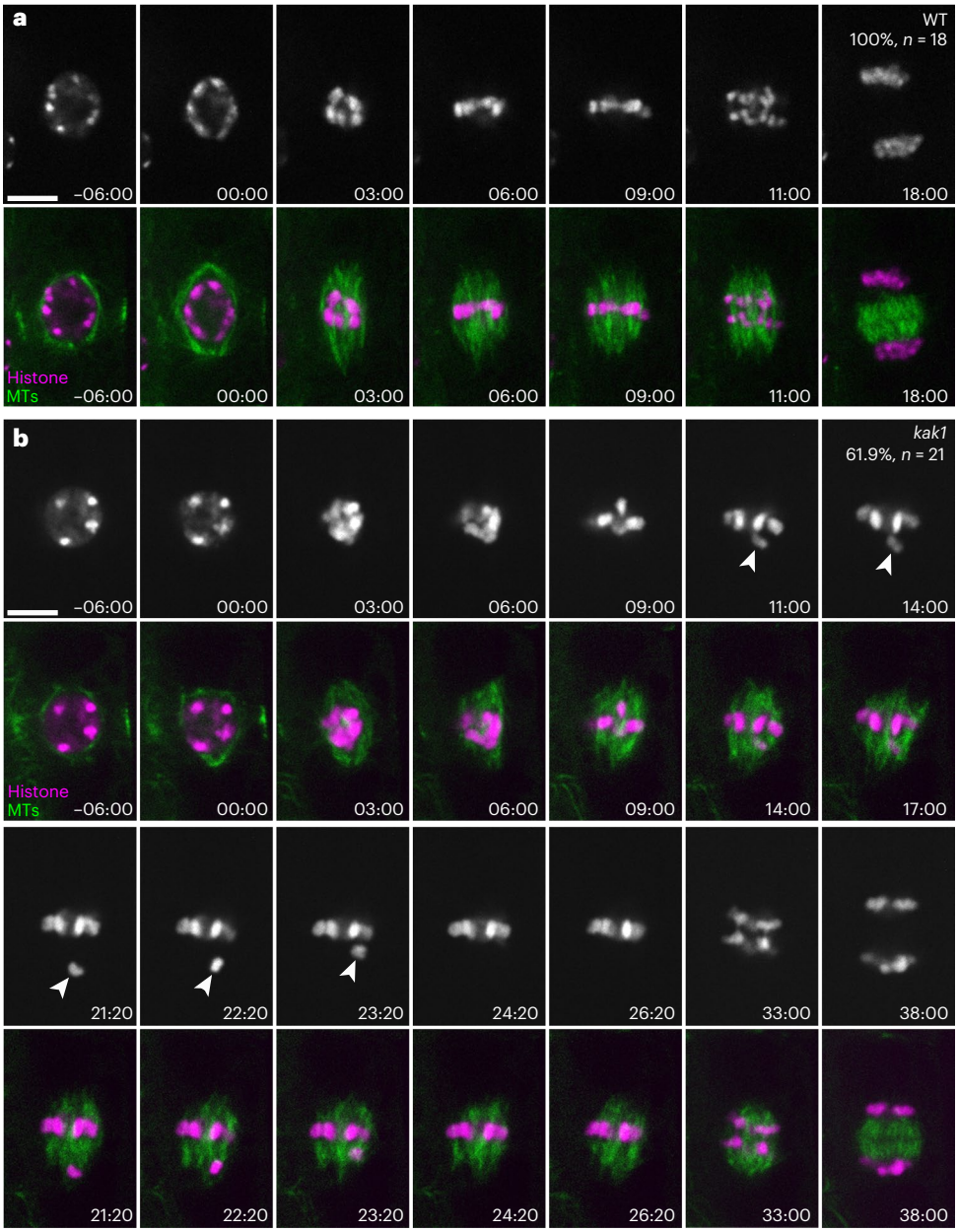

Fig. 2 | KAK1 plays a critical role in mitotic chromosome congression. a, Live-cell imaging of WT plants expressing GFP–TUB6 (green) and histone H1.2–RFP (magenta). Representative snapshot images are from Supplementary Video 1. **b**, Live-cell imaging of *kak1* plants expressing GFP–TUB6 (green) and histone H1.2–RFP (magenta). Images are from Supplementary Video 2. Misaligned chromosomes are indicated by arrowheads. Scale bars, 5 µm.

KAK1 (residues 1–600) containing the IR1 domain. By contrast, KAK1 fragments lacking the IR1 domain did not show any interaction with GST–BUB3.3 (Extended Data Fig. 3). Collectively, these results demonstrate that the IR1 domain in the stalk region of KAK1 is required for its binding to BUB3.3.

KAK1 and BUB3.3 show interdependent kinetochore localization

Our finding that KAK1 interacts with BUB3.3 led us to further investigate the relationship between these two proteins in terms of their kinetochore localization during mitosis. To test this, we transformed *pKAK1*::KAK1–GFP into the *bub3.3* mutant background and examined the subcellular localization of KAK1–GFP during mitosis. In control cells, the KAK1–GFP fusion protein exhibited robust kinetochore localization and was able to rescue the chromosome alignment defects observed in the *kak1* mutant plants (Fig. 4a). However, in *bub3.3* cells, the KAK1–GFP signal was mainly detected on the spindle apparatus and in the cytoplasm, but was conspicuously absent from the kinetochores, even on the misaligned chromosomes (Fig. 4b).

We then tested whether KAK1 conversely is needed for BUB3.3 kinetochore targeting. When a functional GFP–BUB3.3 construct was expressed in the *bub3.3* mutant, it was properly associated with the kinetochores, as demonstrated previously[21] (Fig. 4c). However, in *kak1* mutant plants, the GFP–BUB3.3 signal exhibited a diffuse cytoplasmic localization, with no accumulation at the kinetochores of either aligned or misaligned chromosomes (Fig. 4d). Western blot analysis confirmed that the protein levels of KAK1–GFP and GFP–BUB3.3 were not affected in the *bub3.3* and *kak1* mutant backgrounds, respectively (Supplementary Fig. 4). Taken together, these results demonstrate an interdependent relationship between KAK1 and BUB3.3, whereby they rely on each other for their proper localization to the kinetochores during mitosis.

https://doi.org/10.1038/s41477-024-01824-7

a

Bait	Detected proteins			
	BUB3.3		KAK1	
	Peptides (*n*)	Coverage (%)	Peptides (*n*)	Coverage (%)
GFP–BUB3.3	14	54.1	85	60.7
KAK1–GFP	15	52.2	86	61.6
GFP	0	0	0	0

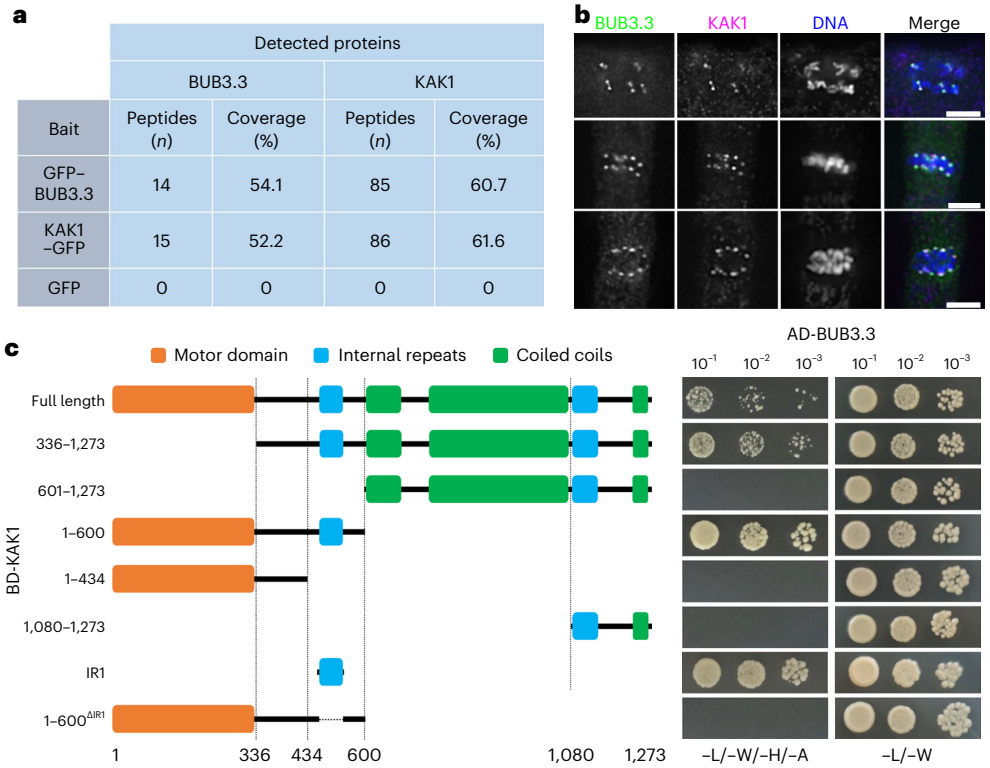

Fig. 3 | KAK1 interacts with BUB3.3. a, Co-purification of BUB3.3 and KAK1 as examined by MS-assisted peptide identification. The number of unique peptides (peptides) and sequence coverage (coverage) are listed. **b**, Immunolocalization images of GFP–BUB3.3 (green), KAK1–FLAG (magenta) and DNA (blue) during mitosis. Micrographs are representative of more than 60 cells from three independent lines with similar results. Scale bars, 5 µm. **c**, Assessment of interactions between BUB3.3 and KAK1 variants by Y2H assay. Schematic representation of full-length and truncated versions of KAK1 used to map BUB3.3-binding domains via the Y2H assay. KAK1 domains are predicted using the SMART bioinformatics tool, and different domains are indicated in the coloured boxes. Yeast cultures are diluted to A600 values of 10^{-1}, 10^{-2} and 10^{-3}, then spotted on vector-selective (−L/−W) and interaction-selective (−L/−W/−H/−A) media. The experiment was repeated three times with similar results. AD, activation domain; BD, binding domain.

SAC defects in *kak1* plants causes chromosome missegregation

Although the *kak1* mutant cells frequently exhibited chromosome alignment defects during metaphase, the onset of anaphase was arrested until proper chromosome congression was achieved (Fig. 2b). This suggested the SAC remained functionally intact in *kak1* plants. By contrast, SAC signalling is known to be disrupted in *bub3.3* plants, which often proceed through anaphase despite the presence of misaligned chromosomes, as reported previously[21]. Based on these differences, we propose that KAK1 may facilitate chromosome congression through a mechanism that is separate from SAC activity. In support of this hypothesis, we found that, whereas more than 60% of *kak1* metaphase cells displayed congression errors, missegregated chromosomes were hardly observed during anaphase (Extended Data Fig. 2). Conversely, in the *bub3.3* mutant, the defective SAC activity led to misaligned chromosomes being present in 26.7% of the anaphase cells (Extended Data Fig. 4). Intriguingly, other known SAC mutants, such as *mps1*, *bmf1*, *bmf2* *bmf3*, *mad1* and *mad2* (ref. 24), did not exhibit noticeable uncongressed chromosomes at both metaphase and anaphase (Extended Data Fig. 4).

To further investigate whether the differential chromosome segregation phenotypes observed between the *kak1* and *bub3.3* mutants could be attributed to their relative impacts on the SAC pathway, we introduced a *Mitotic Arrest Deficient 1* (*MAD1*) mutation into the *kak1* mutant to perturb SAC signalling. Unlike the previously reported lethality of the *bub3.3 mad1* combination[25], the *kak1 mad1* plants were viable and grew normally (Extended Data Fig. 5). However, the double mutant exhibited enhanced sensitivity to oryzalin treatment when compared with the single *kak1* and *mad1* mutants (Extended Data Fig. 6). Live-cell imaging revealed that the double mutant bypassed the 'wait-and-align' behaviour seen in the *kak1* single mutant, with 27.3% ($n = 22$) of mitotic cells undergoing premature anaphase with misaligned chromosomes at the spindle poles (Fig. 5b and Supplementary Video 4). This chromosome segregation defect was more akin to the *bub3.3* mutant, in which 22.7% ($n = 22$) of mitotic cells underwent anaphase with misaligned chromosomes (Fig. 5c and Supplementary Video 5). By contrast, the *mad1* single mutant did not display chromosome congression problems during mitosis (0%, $n = 16$) (Fig. 5a and Supplementary Video 3).

Immunofluorescence analysis for the kinetochore marker centromeric histone H3 (CENH3) further corroborated these findings (Extended Data Fig. 7). Whereas WT plants consistently displayed ten CENH3 foci (corresponding to the *Arabidopsis* chromosome number) in the forming daughter cells at the end of mitosis, the *kak1 mad1* mutant cells (38.2%, $n = 55$) exhibited a distribution of aneuploid chromosome numbers, including 9 + 11 or 8 + 12 CENH3 signals. This indicates that the premature anaphase observed in the double mutant leads to the generation of aneuploid daughter cells.

Importantly, we also isolated a *kak1 bub3.3* double mutant, which did not exhibit any overt growth phenotype (Extended Data Fig. 5), and live-cell imaging analysis showed that the *kak1 bub3.3* mutant did not exhibit more severe chromosome congression or segregation problems when compared with the *bub3.3* single mutant (Fig. 5d and Supplementary Video 6). In addition, similar to the *bub3.3* mutant, the kinetochore localization of SAC proteins like BUB1/MAD3 family protein 3 (BMF3) and MAD1 appeared unaltered in the *kak1* mutant (Extended Data Fig. 8). Taken together, these findings indicate that KAK1 may function in the same pathway as BUB3.3 to regulate chromosome congression,

https://doi.org/10.1038/s41477-024-01824-7

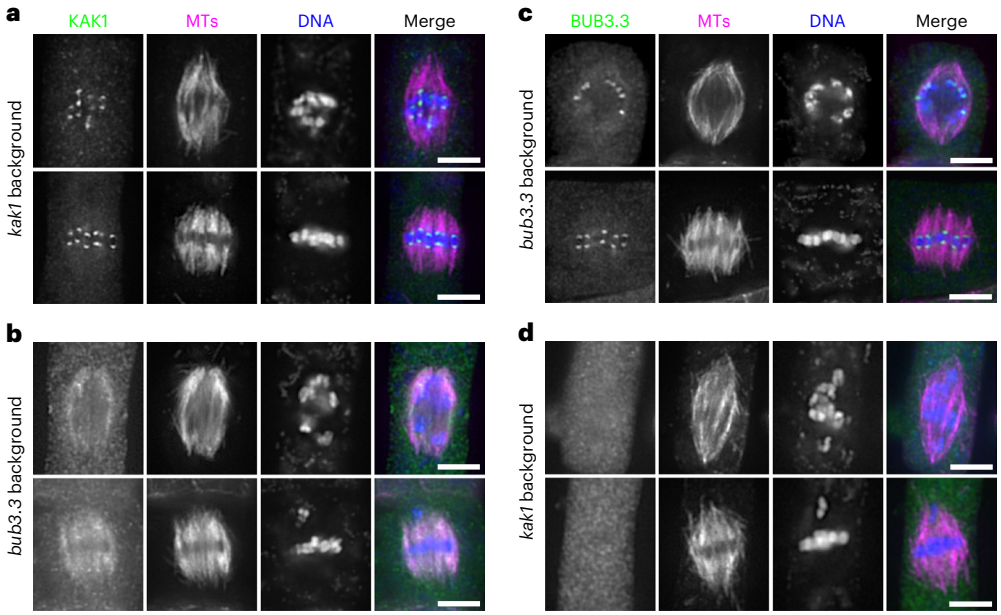

Fig. 4 | KAK1 and BUB3.3 exhibit interdependent kinetochore localization. **a**,**b**, KAK1–GFP localization upon expression in *kak1* (**a**) and *bub3.3* (**b**) mutant backgrounds. **c**,**d**, GFP–BUB3.3 localization in *bub3.3* (**c**) and *kak1* (**d**) mutant backgrounds. The fluorescent signals are detected using immunofluorescence microscopy, with GFP-tagged KAK1 or BUB3.3 detected by anti-GFP shown in green, MTs detected by anti-tubulin shown in magenta, and DNA detected by DAPI shown in blue. Micrographs are representative of more than 60 cells from three independent lines with similar results. Scale bars, 5 µm.

but unlike BUB3.3, KAK1 is unlikely to be a critical component of the canonical SAC machinery.

Mitotic chromosome congression requires KAK1 motor activities

Our transient expression experiments in tobacco leaves demonstrated that the motor domain of KAK1 is capable of binding to microtubules (Supplementary Fig. 5). To further assess the contribution of KAK1's motor domain to its mitotic functions, we generated KAK1 variants lacking the motor domain (KAK1$^{\Delta M}$) or harbouring a T86N point mutation at the motor domain that abolishes ATP binding (KAK1^{T86N}). We expressed both KAK1 variants in *kak1* seedlings using the native *KAK1* promoter and found that neither variant could rescue the oryzalin hypersensitivity of *kak1* seedlings, as quantified by reduced root growth when compared with KAK1 complementary lines (Fig. 6a,b). Interestingly, when expressed in *kak1* plants, GFP-tagged KAK1$^{\Delta M}$ and KAK1^{T86N} still concentrated robustly at kinetochores, similarly to the unmodified KAK1 protein (Fig. 6c,e). Notably, although KAK1 fully rescued chromosome congression defects in *kak1* plants, more than 60% of *kak1* metaphase cells expressing the KAK1$^{\Delta M}$ and KAK1^{T86N} variants showed misaligned chromosomes (Fig. 6c,e). Thus, the motor activity of KAK1 is essential for ensuring chromosome congression, but not for its kinetochore localization.

Because KAK1 is required to generate forces on mono-oriented chromosomes to drive their congression to the cell equator, we hypothesize that the loss of KAK1 from kinetochores could be the cause of the chromosome congression failure observed in *bub3.3* plants. To test this, we engineered fusion proteins of KAK1 and BUB3.3 with the C-terminal kinetochore-targeting sequence of the kinetochore scaffold 1 (KNL1) protein. Both KNL1^{C}–BUB3.3 and KAK1–KNL1^{C} localized to kinetochores when expressed in their respective mutant lines and successfully rescued the chromosome misalignment phenotypes (Supplementary Fig. 6), confirming that they retained normal activities. Strikingly, KAK1–KNL1^{C} was able to localize to kinetochores in the *bub3.3* mutant background, where unmodified KAK1 normally loses its kinetochore association without BUB3.3 (Fig. 7a). Importantly, artificial tethering of KAK1 to kinetochores was sufficient to suppress the growth retardation caused by oryzalin treatment in *bub3.3* plants (Fig. 7b). Quantitative analysis revealed a substantial reduction in the frequency of misaligned chromosomes in *bub3.3* mutant cells expressing KAK1–KNL1^{C} (Fig. 7g). By contrast, targeting BUB3.3 to kinetochores by fusing it with KNL1^{C} could not rescue the frequent polar chromosomes and oryzalin-induced growth defects in *kak1* plants (Fig. 7d–g). Thus, artificially restoring KAK1, but not BUB3.3, at kinetochores bypassed requirements for their interdependent recruitment and functionally complemented chromosome alignment failures.

Collectively, these domain-swap experiments place KAK1 downstream of BUB3.3 for its role in chromosome congression. Our findings indicate that BUB3.3 is required to recruit KAK1 to kinetochores, but the presence of BUB3.3 alone is not sufficient for proper chromosome congression. Rather, KAK1's motor activity and the forces it generates on mono-oriented chromosomes appear to be essential for achieving metaphase plate alignment.

Discussion

In this Article, we identify KAK1 as a kinetochore-associated kinesin that interacts with BUB3.3 and is essential for proper chromosome congression in *Arabidopsis*. Although KAK1 has functional similarities to animal CENP-E as a microtubule-based motor that transports chromosomes to the metaphase plate, our findings reveal KAK1 utilizes distinct binding partners and action modes to fulfil its function in *Arabidopsis*. Thus, plants have evolved connections between chromosome bi-orientation and SAC activity through specialized architecture design at their kinetochores. Our elucidation of KAK1's function mechanism advances understanding of the intricate pathways governing mitotic fidelity in plant systems.

Despite the relatively conserved kinesin-like motor domain shared between KAK1 and the animal CENP-E protein, the two proteins exhibit substantial divergence in their non-motor regions. A key distinction is the absence of the common kinetochore-targeting domain found in the C-terminal tail of CENP-E[7], which is lacking in the KAK1 sequence. This structural difference probably contributes to the distinct kinetochore localization patterns observed between KAK1 and CENP-E during mitosis. In animal cells, CENP-E is specifically recruited to kinetochores

https://doi.org/10.1038/s41477-024-01824-7

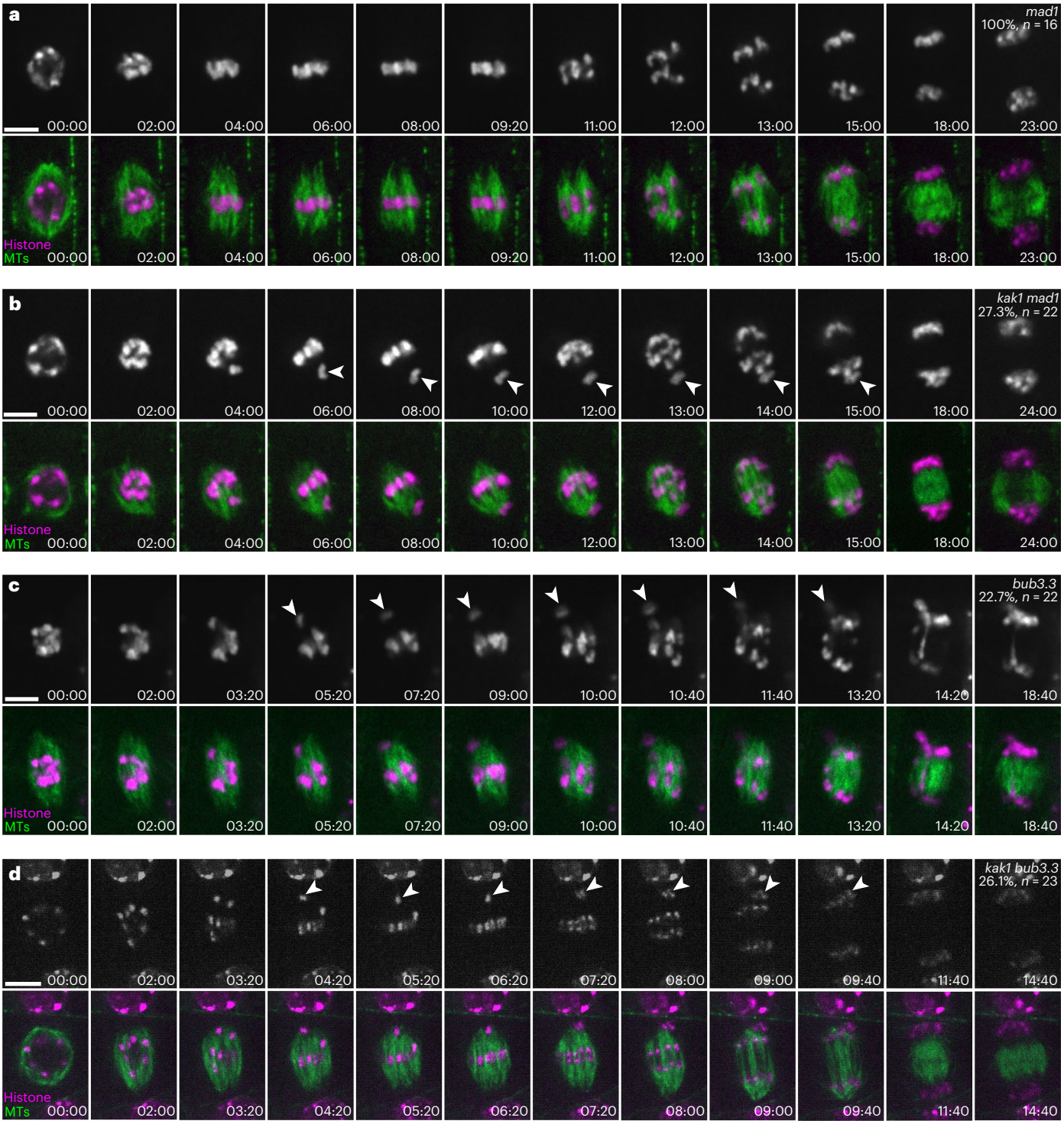

Fig. 5 | Inhibition of SAC in *kak1* plants leads to chromosome missegregation. **a**, Live-cell imaging of *mad1* mutant plants expressing GFP–TUB6 (green) and histone H1.2–RFP (magenta). Representative snapshot images are from Supplementary Video 3. **b**, Live-cell imaging of *kak1 mad1* double-mutant plants expressing GFP–TUB6 (green) and histone H1.2–RFP (magenta). Images are from Supplementary Video 4. **c**, Live-cell imaging of *bub3.3* mutant plants expressing GFP–TUB6 (green) and histone H1.2–RFP (magenta). Representative snapshot images are from Supplementary Video 5. **d**, Live-cell imaging of *kak1 bub3.3* double-mutant plants expressing GFP–TUB6 (green) and histone H1.2–RFP (magenta). Images are from Supplementary Video 6. Arrowheads indicate misaligned chromosomes. Scale bars, 5 µm.

at early mitosis and then degraded after metaphase[26,27]. By contrast, our data show that KAK1 associates with kinetochores throughout the entire mitotic process. This divergence in kinetochore binding dynamics may be attributed to differences in the adaptor proteins that mediate the localization of these kinesins. In animals, CENP-E is known to directly interact with BUBR1, which acts as the primary recruiter of CENP-E to kinetochores during chromosome alignment and SAC activation[10,28]. However, our work in plants demonstrates that the BUB3.3 protein functions as the key kinetochore recruiter for KAK1. Unlike the transient association of BUBR1 with kinetochores, the plant-specific BUB3.3 protein remains associated with kinetochores throughout mitosis[21]. This differential kinetochore binding behaviour

https://doi.org/10.1038/s41477-024-01824-7

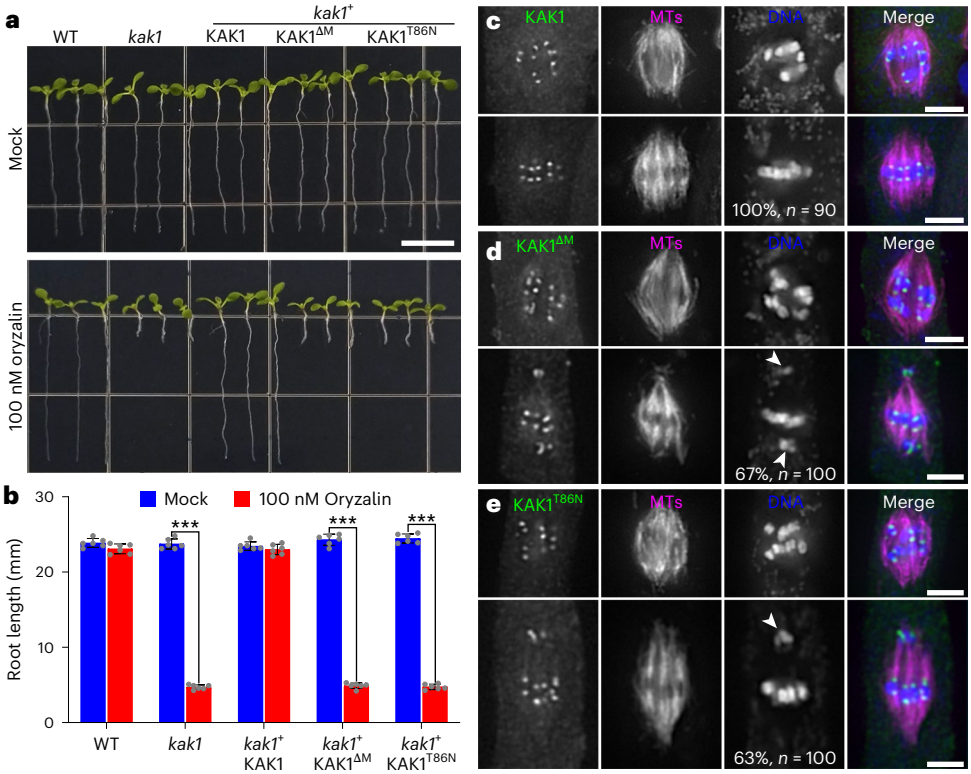

Fig. 6 | KAK1 ensuring chromosome congression requires its motor activity. **a**, Growth phenotypes of 10-day-old seedlings expressing KAK1, the motor domain deleted KAK1$^{\Delta M}$ and the motor activity-defective KAK1^{T86N} variants with and without 100 nM oryzalin treatment. Scale bars, 1 cm. **b**, Quantification of root lengths in seedlings with and without oryzalin treatment. Bars represent means ± s.d. of six seedlings per genotype. Statistical significance (***$P < 10^{-6}$) was determined by one-way ANOVA with post-hoc Tukey's test. The experiment was repeated three times with similar results. **c**–**e**, Localization of KAK1 (**c**), KAK1$^{\Delta M}$ (**d**) and KAK1^{T86N} (**e**) in the *kak1* mutant background. The fluorescent signals are detected by immunofluorescence and merged images have GFP-tagged proteins detected by anti-GFP shown in green, MTs detected by anti-tubulin shown in magenta and DNA detected by DAPI shown in blue. Arrowheads indicate misaligned chromosomes. Micrographs are representative of at least 90 cells from three independent lines with similar results. Scale bars, 5 µm.

probably contributes to the persistent localization of KAK1 at the kinetochores compared with the more dynamic recruitment of CENP-E.

The direct interaction between KAK1 and BUB3.3 provides molecular insights into how plants coordinate chromosome alignment and SAC signalling at kinetochores. In animal cells, CENP-E not only regulates chromosome congression, but is also thought to play a crucial role in SAC activation[17]. CENP-E has been shown to interact with multiple SAC components, including BUBR1 and MAD1 (ref. 29), and can even mediate the activation and autophosphorylation of the BUBR1 kinase[11,30,31]. The phosphorylated form of BUBR1 can then directly inhibit the anaphase-promoting complex/cyclosome by reducing the association of the MAD1–MAD2 complex at unattached kinetochores[32]. Thus, CENP-E is considered to be a key player in SAC signalling via this BUBR1-dependent pathway. By contrast, our findings suggest that KAK1 does not appear to be a critical component of the core SAC machinery in plants. Although the *kak1* mutant cells exhibit widespread chromosome misalignment at metaphase, these cells are still largely able to arrest at this stage, preventing premature anaphase entry. This is in contrast to the *bub3.3* mutant, which displays frequent anaphase segregation defects indicative of a compromised SAC.

Our previous work has demonstrated that BUB3.3 has core functions in SAC activation through interacting with BMF3 to recruit the protein cell division cycle 20 (CDC20)[21]. Here we further reveal that BUB3.3 also plays a critical role in the process of chromosome congression, achieved through its ability to tether the KAK1 motor to kinetochores. It is intriguing that in the absence of KAK1, BUB3.3 also fails to localize to kinetochores. This finding is somewhat unexpected, given that our domain-swap experiments revealed that KAK1 functions as a kinesin motor downstream of BUB3.3 for aligning chromosomes. We propose that BUB3.3 and KAK1 may first form a cytoplasmic complex before being recruited to kinetochores. When mitosis is initiated, this preformed BUB3.3–KAK1 complex is then targeted to kinetochores.

Even though the kinetochore localization of BUB3.3 requires KAK1, we propose that BUB3.3 may be able to interact with BMF3 in the cytoplasm, even in the absence of KAK1-mediated recruitment. This potential cytoplasmic interaction could support continued formation of the mitotic checkpoint complex containing CDC20, thereby leading to the metaphase arrest phenotype observed in the *kak1* mutant. By contrast, the *bub3.3* mutant, which lacks this BUB3.3–BMF3 interaction altogether, is unable to properly activate the SAC[21]. Interestingly, disrupting SAC signalling through loss of MAD1 in *kak1* plants causes precocious anaphase onset with misaligned chromosomes, which is reminiscent of the anaphase phenotype in *bub3.3* plants. This genetic interaction indicates that KAK1 and the SAC (at least MAD1) cover complementary branches of mitotic regulation governed by BUB3.3. Furthermore, the viability of *kak1 mad1* plants versus the lethality of *bub3.3 mad1* plants[25] highlights the essential nature of BUB3.3 at the core of multiple control pathways ensuring chromosome segregation fidelity.

Our research also indicates that plants have developed distinct strategies in coordinating the complex regulatory networks governing faithful chromosome segregation at kinetochores, which are unlike any previously known canonical pathways. This probably reflects the rapid evolution of kinetochore components in plants compared with other eukaryotes[33,34]. Although the core scaffolding roles are maintained among plant kinetochore proteins, variations in protein interaction motifs and signalling mechanisms have led to divergent functional wiring[35]. For example, in animal cells, the BUB3 protein always interacts

https://doi.org/10.1038/s41477-024-01824-7

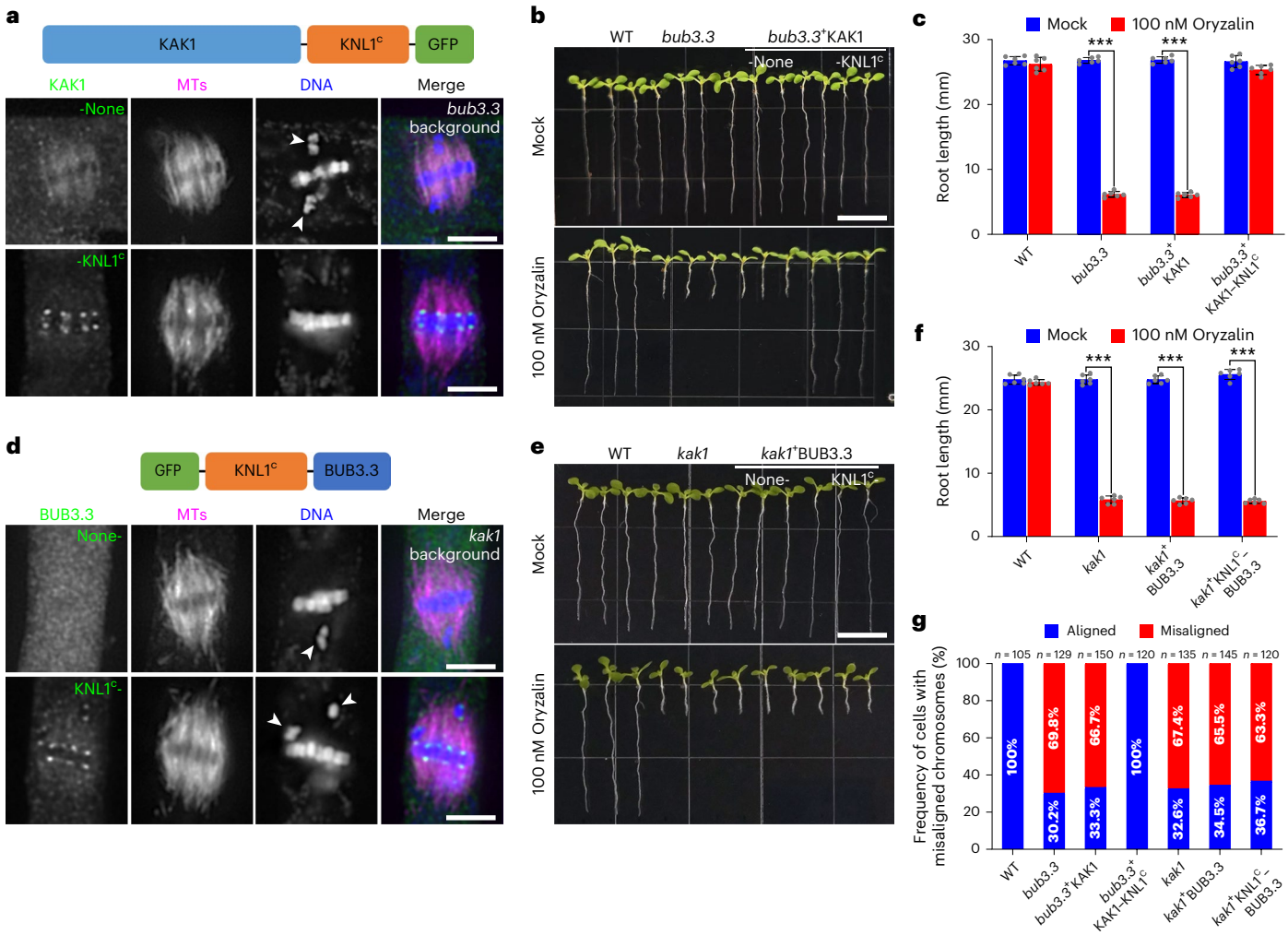

Fig. 7 | KAK1 functions downstream of BUB3.3 at kinetochores for mitotic chromosome congregation. a, Localization of KAK1–GFP and KAK1–KNL1^{C}–GFP in the *bub3.3* mutant background. The fluorescent signals are detected by immunofluorescence and merged images have GFP-tagged proteins detected by anti-GFP shown in green, MTs detected by anti-tubulin shown in magenta, and DNA detected by DAPI shown in blue. Arrowheads indicate misaligned chromosomes. **b**, Growth comparison of 10-day-old seedlings of WT, *bub3.3* and *bub3.3*-expressing KAK1 derivatives with and without 100 nM oryzalin treatment. **c**, Quantification of root lengths in the seedlings shown in **b**, values are means ± s.d. from six seedlings per genotype. Asterisks indicate notable differences determined by one-way ANOVA with Tukey test (***$P < 10^{-6}$). **d**, Immunofluorescence localization of GFP–BUB3.3 and GFP–KNL1^{C}–BUB3.3 in the *kak1* mutant background. Arrowheads indicate misaligned chromosomes. **e**, Growth comparison of 10-day-old seedlings of WT, *kak1* and *kak1*-expressing BUB3.3 derivatives with and without 100 nM oryzalin treatment. **f**, Quantification of root lengths in the seedlings shown in **e**, values are means ± s.d. from six seedlings per genotype, and the asterisks indicate statistically differences (one-way ANOVA with Tukey test, ***$P < 10^{-6}$). **g**, Quantitative assessment of metaphase cells exhibiting misaligned chromosomes in different plants. Scale bars, 5 µm (**a**,**d**), 1 cm (**b**,**e**). The data are representative of three independent experiments with similar results.

with BUB1 and BUBR1 proteins containing the Gle2-binding sequence domain, as well as the kinetochore scaffold protein KNL1, by recognizing the phosphorylated Met-Glu-Leu-Thr motifs[3,4]. However, these canonical interaction modes observed in animal systems may not apply directly to flowering plants, because the plant-specific BMF and KNL1 proteins do not share the Gle2-binding sequence and Met-Glu-Leu-Thr domains[36]. Instead, several recent studies have revealed that plants established alternative interaction domains and modules to assemble similar molecular complex at kinetochores. For instance, in *Arabidopsis*, the KNL1 protein evolves a eudicot-specific domain that can independently recruit the BUB3.3 and BMF3 proteins to kinetochores[37,38], and BUB3.3 specifically binds to BMF3 via two IR motifs[21]. Interestingly, BUB3.3 also builds an interaction with the KAK1 kinesin through an IR domain within the KAK1 stalk region. Notably, the two IR domains within the KAK1 stalk display relatively low sequence similarity. This suggests that the IR1 and IR2 domains of KAK1 may have divergent functions, which could explain why only the IR1 domain is required for binding to BUB3.3, whereas the IR2 domain does not contribute to this interaction. Importantly, there is also no sequence similarity between the IR regions of KAK1 and those found in the BMF3 protein. These observations suggest that the *Arabidopsis* BUB3.3 protein has the ability to recognize and bind to different types of IR motifs present in various kinetochore proteins. However, the precise mechanisms by which plant BUB3.3 reads and discriminates between the distinct IRs remains an intriguing open question. Overall, the alternative architectures observed from the plant-specific orthologues of KNL1, BMFs, BUB3 and KAK1 suggest that the protein interactions and connections at the kinetochore interface have been tailored specifically to the plant lineage. Ongoing identification of new kinetochore-associated proteins in plants will help reconstruct the architectural blueprints that are specific to the plant kingdom. Ultimately, determining how conserved scaffolds are adapted in distinct lineages will provide key evolutionary insights into the plasticity of cell division mechanisms across eukaryotes.

Although the KAK1 protein is essential for efficient chromosome congression, our findings indicate that additional proteins probably cooperate with KAK1 to ensure proper movement of chromosomes. We observe that the *kak1* mutant cells can eventually achieve full metaphase plate alignment of chromosomes, albeit after a delay, suggesting the existence of redundant mechanisms for chromosome congression. In animals, a coordinated ensemble of motor proteins, including dynein and various kinesins such as CENP-E, kinesin-4, kinesin-10 and kinesin-13, act together to steer chromosome movements along the spindle microtubules[39–43]. Although plants lack the dynein motor, they possess multiple kinesin families whose mitotic functions remain largely unexplored[18,44]. Identifying potential kinetochore-associated partners that act in conjunction with KAK1 will provide key insights into robust chromosome transport mechanisms used in plants. For instance, are there complementary microtubule motors that can take over when the KAK1 function is disrupted? Or are there adaptor proteins that can bridge KAK1 to the microtubule lattice or plus ends? Elucidating these questions will enhance understanding of the remarkable adaptability and built-in redundancy of plant cell division control pathways.

In summary, our study defines the essential role of KAK1 in chromosome congression and reveals unique regulatory strategies used at plant kinetochores. Further investigation into the regulation and microtubule coupling mechanisms of KAK1 will provide deeper insights into the chromosome congression mechanisms in plants. A particularly important question to address is how KAK1 integrates chromosome alignment signals with its own motor activity. It will be intriguing to elucidate whether there are any post-translational modifications, such as phosphorylation events, involved in the regulation of KAK1's motor activity, analogous to the Aurora kinase-dependent pathways observed in animal cells[45,46]. Unravelling these molecular details will advance our understanding of how the intricate protein machinery assembled at plant kinetochores enables the dynamic yet accurate movements of chromosomes during cell division.

Methods

Plant materials and growth conditions

Arabidopsis thaliana ecotype Columbia (Col) was used as the WT control in this study. The *kak1* mutant was isolated from the seed stock of SALK_115677, which was obtained from the *Arabidopsis* Biological Research Center at Ohio State University. The *bub3.3* (SALK_022904) mutant was described previously[21]. All plants were grown in an environmentally controlled chamber under a 16 h light and 8 h dark cycle at 22 °C. *Agrobacterium tumefaciens* strain GV3101 was used for floral dipping-based transformation in *Arabidopsis*. Seedlings for live-cell imaging and immunolocalization experiments were produced on solid medium containing 1/2 Murashige Skoog basal medium and 0.8% phytagel.

For genotyping of the *kak1* mutant, kak1-LP (CTTAAAATAGCATGACAAAAGGGG) and kak1-RP (TTGCAGGTATTATCCAATGTTTTG) were used for amplification of the *KAK1* allele; kak1-RP and LBb1.3 were used for amplification of the *kak1* allele. Genotyping of *bub3.3* and other *SAC gene* mutants was performed as previously described[21,24].

For oryzalin-sensitivity examination, seeds were germinated on 1/2 Murashige Skoog solid medium supplied with 100 nM oryzalin from 100 mM stock previously dissolved in dimethyl sulfoxide. Plates containing equal volumes of dimethyl sulfoxide were used as the mock control. Seedlings grown on plates with or without oryzalin were photographed and root length was measured by the ImageJ software.

Construction of expression vectors

To produce KAK1–GFP and KAK1–FLAG constructs, a 10,283-bp KAK1 genomic fragment, which contains a 2,034-bp promoter region and deletes the stop codon, was amplified and recombined into the pDONR221 vector using BP clonase (ThermoFisher Scientific). The resulting pENTR-gKAK1 was then recombined with pGWB650 and pGWB610 via LR recombination reactions (ThermoFisher Scientific) to yield C terminus GFP and FLAG fusions. The binary vectors of GFP–BUB3.3, BMF3–GFP, GFP–MAD1, histone H1.2–TagRFP and GFP–TUB6, which were expressed by their native promoters, were described previously[24,47].

All truncations of KAK1 were expressed under the native KAK1 promoter by using the pENTR-gKAK1 plasmid as the template. This backbone was amplified to remove the motor domain or mutate the Thr86 residue to Asn through polymerase chain reaction-based site-directed mutagenesis. These truncated entry vectors are recombined into the pGWB650 vector by LR clonase, to yield a translational fusion with a C terminus GFP. Primer pairs for plasmid construction are listed in Supplementary Table 1.

Protein sequence alignment and phylogenetic analysis

The annotation of each protein sequence was based on information from the *Arabidopsis* Information Resource (https://www.arabidopsis.org/) and UniProt database (https://www.uniprot.org/). Sequence alignment was performed using the ClustalW method in MEGA software, and the aligned sequences were further annotated using Jalview. The conservation levels of the amino acids were evaluated using the BLOSUM62 scoring matrix. Annotations of protein domains and motifs were conducted based on data from the SMART database (http://smart.embl.de/).

For the phylogenetic analysis, the protein sequences were aligned using the MUSCLE method, followed by construction of the phylogenetic tree via the neighbour-joining method in MEGA. Gaps in the aligned sequences were automatically removed by MEGA using the complete-deletion option. The reliability of the phylogenetic tree was assessed through 1,000 bootstrap replicates.

RNA isolation and complementary DNA synthesis

Total RNA was extracted from the flower buds of 5-week-old plants using the MolPure TRIeasy Plus Total RNA Kit (Yeasen Biotechnology, catalogue no. 19211ES) according to the manufacturer's instructions. The extracted RNA was then treated with DNase I to remove any genomic DNA contamination. For cDNA synthesis, approximately 1 µg of purified total RNA was reverse transcribed using the M-MLV Reverse Transcriptase Kit (ThermoFisher Scientific, catalogue no. 28025013) with oligo$(dT)_{18}$.

Yeast two-hybrid assay

For the Y2H assay, the coding sequence of KAK1 was amplified and cloned into pDONR221 via BP clonase. The entry vector containing the KAK1 coding sequence was linearized by polymerase chain reaction to produce truncated KAK1 vectors. The entry vector containing the coding sequence of BUB3.3 was described as published[21]. All the subcloned cDNA entry vectors were recombined into pGADT7-GW (Addgene, catalogue no. 61702) or pGBKT7-GW (Addgene, catalogue no. 61703) via LR recombination reactions. The resulting constructs were transformed into the yeast strain AH109 and were spotted on synthetic dextrose plates without Leu and Trp (−L/−W; control media) or without Leu, Trp, His and Ade (−L/−W/−H/−A; selection media) and photographed after incubation at 30 °C for 2 days.

In vitro protein expression and pull-down assay

For recombinant protein productions, entry clones containing coding sequences of BUB3.3 and KAK1 truncations were recombined into pDEST565 (Addgene, catalogue no. 11520) or pDEST566 (Addgene, catalogue no. 11517) through LR clonase. These plasmids allow expression of GST- or MBP-tagged fusion proteins in the *E. coli* BL21 host strain. The fusion proteins were purified using glutathione HiCap matrix (Qiagen, catalogue no. 30900) or MBPSep dextrin agarose resins (Yeasen Biotechnology, catalogue no. 20515ES) according to the manufacturer's instructions.

For pull-down assays, MBP or MBP-fused truncated KAK1 proteins were incubated with equal amounts of GST-tagged BUB3.3 immobilized on glutathione resins. Protein binding reactions were performed in 1× TBST buffer (20 mM Tris–HCl pH 8.0, 150 mM NaCl, 0.2% Triton X-100) at 4 °C for 2 h with gently rotation. After washing five times with 1× TBST, the resins were collected by centrifugation at 5,000*g* for 1 min. Bound proteins were boiled in 50 µl of 1× sodium dodecyl sulfate (SDS) sample buffer for 10 min at 100 °C, then separated by SDS–polyacrylamide gel electrophoresis and transferred to a polyvinylidene difluoride membrane. The membrane was washed with 1× TBST, and primary antibodies diluted in 1× TBS buffer (20 mM Tris–HCl pH 8.0, 150 mM NaCl, 0.2% Triton X-100) were added to the membrane for a 3-h incubation. The primary antibodies used were mouse anti-MBP immunoglobulin G (IgG) and mouse anti-GST IgG (1:10,000, GenScript, catalogue nos. A00190 and A00865). After washing the membrane with 1× TBST, it was incubated for 1 h with secondary horseradish peroxidase-conjugated goat anti-mouse IgG (1:10,000, ThermoFisher Scientific, catalogue no. 31430) diluted in 1× TBS. Finally, the membrane was washed with 1× TBST, and the chemiluminescence was detected using an ECL Chemiluminescent Substrate Kit (Yeasen Biotechnology, catalogue no. 36222)

Affinity purification and mass spectrometry

Proteins were extracted from control *Arabidopsis* plants and transform plants expressing the GFP fusions with KAK1 and BUB3.3. In brief, flower buds from 5-week-old plants were frozen in liquid nitrogen and ground to powder using a mortar and pestle. An extraction buffer containing 50 mM Tris–HCl, pH 8.0, containing 150 mM NaCl and 1% Triton X-100 was added to the powder and incubated at 4 °C for 1 h. The supernatant was collected after centrifugation at 15,000*g* and filtration through a 5-µm syringe filter (PALL, catalogue no. 4650). The GFP fusion proteins were purified with GFP antibody-conjugated magnetic beads according to the manufacturer's instructions (Miltenyi Biotecm, catalogue no. 130-091-125) and subjected to SDS–polyacrylamide gel electrophoresis with 10% polyacrylamide gels.

To identify co-purified proteins, the gels were stained with PageBlue protein staining solution (ThermoFisher Scientific, catalogue no. 24620) and the stained bands were then excised from the gels and subjected to in-gel trypsin digestion. This involved incubating the gel pieces with sequencing-grade modified trypsin at 37 °C for 16 h to enzymatically break down the proteins into peptides. The resulting peptide mixture contained phosphorylated peptides that were analysed using liquid chromatography tandem MS by Shanghai Luming Biological Technology Co., Ltd.

Immunolocalization and fluorescence microscopy

For immunofluorescence staining experiments, root tips containing meristematic zones were collected from 5-day-old *Arabidopsis* seedlings and fixed for 45 min at room temperature in PME buffer (50 mM PIPES, pH 6.9, 5 mM $MgSO_4$, 1 mM EGTA and 4% formaldehyde). Fixed tissues were washed three times in PME buffer, treated for 15 min with 1% cellulase (Onozuka RS, Yakult) and squashed onto slides. Fixed cells on slides were incubated for 15 min in PME buffer with 0.5% Triton X-100 followed by 10 min in methanol. Fixed cells were then incubated overnight at 4 °C with primary antibodies including GFP recombinant rabbit monoclonal antibody (1:500, ThermoFisher Scientific, catalogue no. G10362), DM1A mouse anti-α-tubulin monoclonal antibody (1:1,000, Abcam, catalogue no. ab7291), 9A3 mouse anti-FLAG monoclonal antibody (1:1,000, Cell Signaling Technology, catalogue no. 8146) and rabbit-anti CENH3 polyclonal antibody (1:500, PhytoAB, catalogue no. PHY7449A) diluted in phosphate-buffered saline containing 3% (w/v) bovine serum albumin. After washing three times in phosphate-buffered saline, secondary antibodies including Alexa Fluor 488-conjugated goat anti-rabbit IgG and Alexa Fluor 555-conjugated goat anti-mouse IgG (1:1,000, ThermoFisher Scientific, catalogue nos. A32731 and A32727) were applied for 2 h at room temperature. Slides were finally mounted with SlowFade Diamond Antifade containing DAPI (ThermoFisher Scientific, catalogue no. S36973). Stained cells were observed under an Eclipse 600 microscope equipped with a ×100 Plan-Apo objective (numerical aperture 1.45, Nikon). The excitation wavelengths used were 364 nm for 4′,6-diamidino-2-phenylindole (DAPI), 488 nm for the Alexa Fluor 488-conjugated secondary antibody and 561 nm for the Alexa Fluor 555-conjugated secondary antibody. The emission filters were set to 420–470 nm for DAPI, 500–550 nm for the Alexa Fluor 488 channel and 570–650 nm for the Alexa Fluor 555 channel. Images were acquired by a panda sCMOS camera (PCO Imaging) and processed in ImageJ.

For live-cell observation, root meristem cells of 5-day-old seedlings were observed using a LSM880 spinning-disk confocal microscope equipped with a ×100 oil-immersion objective (numerical aperture 1.40, Carl Zeiss), with GFP (excitation 488 nm, emission 500–550 nm) and RFP (excitation 561 nm, emission 570–650 nm) filter sets. Time-lapse images were acquired using the ZEN 2 software package (Carl Zeiss) and processed in ImageJ. Figures were assembled in Photoshop CS6 (Adobe) for the final presentation.

Statistical analysis

For all quantitative comparisons between experimental treatments or phenotypes, we performed analysis of variance (ANOVA) tests using GraphPad Prism v.9.0.0 software. The significance of the difference in more than two groups was determined by one-way ANOVA followed by Tukey–Kramer test. The specific *P* values as well as the sample sizes (*n*) for each dataset, are reported directly in the figures or figure legends.

Reporting summary

Further information on research design is available in the Nature Portfolio Reporting Summary linked to this article.

Data availability

All data of this study are available in the main text or the Supplementary Information. Source data are provided with this paper.

References

1. Walczak, C. E., Cai, S. & Khodjakov, A. Mechanisms of chromosome behaviour during mitosis. *Nat. Rev. Mol. Cell Biol.* **11**, 91–102 (2010).
2. Risteski, P., Jagrić, M., Pavin, N. & Tolić, I. M. Biomechanics of chromosome alignment at the spindle midplane. *Curr. Biol.* **31**, R574–R585 (2021).
3. McAinsh, A. D. & Kops, G. J. P. L. Principles and dynamics of spindle assembly checkpoint signalling. *Nat. Rev. Mol. Cell Biol.* **24**, 543–559 (2023).
4. Lara-Gonzalez, P., Pines, J. & Desai, A. Spindle assembly checkpoint activation and silencing at kinetochores. *Semin. Cell Dev. Biol.* **117**, 86–98 (2021).
5. Musacchio, A. The molecular biology of spindle assembly checkpoint signaling dynamics. *Curr. Biol.* **25**, R1002–R1018 (2015).
6. Schaar, B. T., Chan, G. K., Maddox, P., Salmon, E. D. & Yen, T. J. CENP-E function at kinetochores is essential for chromosome alignment. *J. Cell Biol.* **139**, 1373–1382 (1997).
7. Craske, B. & Welburn, J. P. I. Leaving no one behind: how CENP-E facilitates chromosome alignment. *Essays Biochem.* **64**, 313–324 (2020).
8. Wood, K. W., Sakowicz, R., Goldstein, L. S. & Cleveland, D. W. CENP-E is a plus end-directed kinetochore motor required for metaphase chromosome alignment. *Cell* **91**, 357–366 (1997).
9. Chan, G. K., Schaar, B. T. & Yen, T. J. Characterization of the kinetochore binding domain of CENP-E reveals interactions with the kinetochore proteins CENP-F and hBUBR1. *J. Cell Biol.* **143**, 49–63 (1998).

10. Legal, T. et al. The C-terminal helix of BubR1 is essential for CENP-E-dependent chromosome alignment. *J. Cell Sci.* **133**, jcs246025 (2020).
11. Guo, Y., Kim, C., Ahmad, S., Zhang, J. & Mao, Y. CENP-E–dependent BubR1 autophosphorylation enhances chromosome alignment and the mitotic checkpoint. *J. Cell Biol.* **198**, 205–217 (2012).
12. Lampson, M. A. & Kapoor, T. M. The human mitotic checkpoint protein BubR1 regulates chromosome–spindle attachments. *Nat. Cell Biol.* **7**, 93–98 (2005).
13. Iemura, K. & Tanaka, K. Chromokinesin Kid and kinetochore kinesin CENP-E differentially support chromosome congression without end-on attachment to microtubules. *Nat. Commun.* **6**, 6447 (2015).
14. Gudimchuk, N. et al. Kinetochore kinesin CENP-E is a processive bi-directional tracker of dynamic microtubule tips. *Nat. Cell Biol.* **15**, 1079–1088 (2013).
15. Shrestha, R. L. & Draviam, V. M. Lateral to end-on conversion of chromosome–microtubule attachment requires kinesins CENP-E and MCAK. *Curr. Biol.* **23**, 1514–1526 (2013).
16. Mao, Y., Abrieu, A. & Cleveland, D. W. Activating and silencing the mitotic checkpoint through CENP-E-dependent activation/inactivation of BubR1. *Cell* **114**, 87–98 (2003).
17. Yu, K.-W., Zhong, N., Xiao, Y. & She, Z.-Y. Mechanisms of kinesin-7 CENP-E in kinetochore–microtubule capture and chromosome alignment during cell division. *Biol. Cell* **111**, 143–160 (2019).
18. Lee, Y.-R. J., Qiu, W. & Liu, B. Kinesin motors in plants: from subcellular dynamics to motility regulation. *Curr. Opin. Plant Biol.* **28**, 120–126 (2015).
19. Nebenführ, A. & Dixit, R. Kinesins and myosins: molecular motors that coordinate cellular functions in plants. *Annu. Rev. Plant Biol.* **69**, 329–361 (2018).
20. Miki, T., Naito, H., Nishina, M. & Goshima, G. Endogenous localizome identifies 43 mitotic kinesins in a plant cell. *Proc. Natl Acad. Sci. USA* **111**, E1053–E1061 (2014).
21. Deng, X. et al. The *Arabidopsis* BUB1/MAD3 family protein BMF3 requires BUB3.3 to recruit CDC20 to kinetochores in spindle assembly checkpoint signaling. *Proc. Natl Acad. Sci. USA* **121**, e2322677121 (2024).
22. van Leene, J. et al. Targeted interactomics reveals a complex core cell cycle machinery in *Arabidopsis thaliana*. *Mol. Syst. Biol.* **6**, 397 (2010).
23. Shen, Z., Collatos, A. R., Bibeau, J. P., Furt, F. & Vidali, L. Phylogenetic analysis of the Kinesin superfamily from *Physcomitrella*. *Front. Plant Sci.* **3**, 230 (2012).
24. Komaki, S. & Schnittger, A. The spindle assembly checkpoint in *Arabidopsis* is rapidly shut off during severe stress. *Dev. Cell* **43**, 172–185 (2017).
25. Lampou, K., Böwer, F., Komaki, S., Köhler, M. & Schnittger, A. A cytological and functional framework of the meiotic spindle assembly checkpoint in *Arabidopsis thaliana*. Preprint at *bioRxiv* https://doi.org/10.1101/2023.05.26.542430 (2023).
26. Brown, K. D., Wood, K. W. & Cleveland, D. W. The kinesin-like protein CENP-E is kinetochore-associated throughout poleward chromosome segregation during anaphase-A. *J. Cell Sci.* **109**, 961–969 (1996).
27. Howell, B. J. et al. Cytoplasmic dynein/dynactin drives kinetochore protein transport to the spindle poles and has a role in mitotic spindle checkpoint inactivation. *J. Cell Biol.* **155**, 1159–1172 (2001).
28. Johnson, V. L., Scott, M. I. F., Holt, S. V., Hussein, D. & Taylor, S. S. Bub1 is required for kinetochore localization of BubR1, Cenp-E, Cenp-F and Mad2, and chromosome congression. *J. Cell Sci.* **117**, 1577–1589 (2004).
29. Akera, T., Goto, Y., Sato, M., Yamamoto, M. & Watanabe, Y. Mad1 promotes chromosome congression by anchoring a kinesin motor to the kinetochore. *Nat. Cell Biol.* **17**, 1124–1133 (2015).
30. Mao, Y., Desai, A. & Cleveland, D. W. Microtubule capture by CENP-E silences BubR1-dependent mitotic checkpoint signaling. *J. Cell Biol.* **170**, 873–880 (2005).
31. Weaver, B. A. A. et al. Centromere-associated protein-E is essential for the mammalian mitotic checkpoint to prevent aneuploidy due to single chromosome loss. *J. Cell Biol.* **162**, 551–563 (2003).
32. Putkey, F. R. et al. Unstable kinetochore–microtubule capture and chromosomal instability following deletion of CENP-E. *Dev. Cell* **3**, 351–365 (2002).
33. Kozgunova, E., Nishina, M. & Goshima, G. Kinetochore protein depletion underlies cytokinesis failure and somatic polyploidization in the moss *Physcomitrella patens*. *Elife* **8**, e43652 (2019).
34. Tromer, E. C., van Hooff, J. J. E., Kops, G. J. P. L. & Snel, B. Mosaic origin of the eukaryotic kinetochore. *Proc. Natl Acad. Sci. USA* **116**, 12873–12882 (2019).
35. Liu, B. & Lee, Y.-R. J. Spindle assembly and mitosis in plants. *Annu. Rev. Plant Biol.* **73**, 227–254 (2022).
36. Komaki, S. & Schnittger, A. The spindle checkpoint in plants–a green variation over a conserved theme? *Curr. Opin. Plant Biol.* **34**, 84–91 (2016).
37. Su, H. et al. Knl1 participates in spindle assembly checkpoint signaling in maize. *Proc. Natl Acad. Sci. USA* **118**, e2022357118 (2021).
38. Deng, X. et al. A coadapted KNL1 and spindle assembly checkpoint axis orchestrates precise mitosis in *Arabidopsis*. *Proc. Natl Acad. Sci. USA* **121**, e2316583121 (2024).
39. Sharp, D. J., Rogers, G. C. & Scholey, J. M. Cytoplasmic dynein is required for poleward chromosome movement during mitosis in *Drosophila* embryos. *Nat. Cell Biol.* **2**, 922–930 (2000).
40. Yang, Z., Tulu, U. S., Wadsworth, P. & Rieder, C. L. Kinetochore dynein is required for chromosome motion and congression independent of the spindle checkpoint. *Curr. Biol.* **17**, 973–980 (2007).
41. Varma, D., Monzo, P., Stehman, S. A. & Vallee, R. B. Direct role of dynein motor in stable kinetochore–microtubule attachment, orientation, and alignment. *J. Cell Biol.* **182**, 1045–1054 (2008).
42. Wandke, C. et al. Human chromokinesins promote chromosome congression and spindle microtubule dynamics during mitosis. *J. Cell Biol.* **198**, 847–863 (2012).
43. Stumpff, J., Wagenbach, M., Franck, A., Asbury, C. L. & Wordeman, L. Kif18A and chromokinesins confine centromere movements via microtubule growth suppression and spatial control of kinetochore tension. *Dev. Cell* **22**, 1017–1029 (2012).
44. Vanstraelen, M., Inzé, D. & Geelen, D. Mitosis-specific kinesins in *Arabidopsis*. *Trends Plant Sci.* **11**, 167–175 (2006).
45. Kim, Y., Holland, A. J., Lan, W. & Cleveland, D. W. Aurora kinases and protein phosphatase 1 mediate chromosome congression through regulation of CENP-E. *Cell* **142**, 444–455 (2010).
46. Eibes, S. et al. CENP-E activation by Aurora A and B controls kinetochore fibrous corona disassembly. *Nat. Commun.* **14**, 5317 (2023).
47. Deng, X., Xiao, Y., Tang, X., Liu, B. & Lin, H. Arabidopsis α-Aurora kinase plays a role in cytokinesis through regulating MAP65-3 association with microtubules at phragmoplast midzone. *Nat. Commun.* **15**, 3779 (2024).

Acknowledgements

We thank A. Schnittger and S. Komaki for sharing the SAC plasmids and T. Nakagawa for providing pGWB vectors. This study was

supported by the National Natural Science Foundation of China (grant no. 32270354), Natural Science Foundation of Sichuan Province (grant no. 2022NSFSC1651) and Sichuan Forage Innovation Team Program (grant no. SCCXTD-2024-16).

Author contributions

X.D. conceived and supervised the project. X.D., X.T., Y.T. and Y.H. performed most of the experiments. X.D., X.T. and Y.T. analysed the data. X.D. wrote the paper. K.C., H.L. and B.L. read and revised the paper. All authors approved the paper submission.

Competing interests

The authors declare no competing interests.

Additional information

Extended data is available for this paper at https://doi.org/10.1038/s41477-024-01824-7.

Supplementary information The online version contains supplementary material available at https://doi.org/10.1038/s41477-024-01824-7.

Correspondence and requests for materials should be addressed to Xingguang Deng.

Peer review information *Nature Plants* thanks Katharina Bürstenbinder, Ravi Maruthachalam and the other, anonymous, reviewer(s) for their contribution to the peer review of this work.

https://doi.org/10.1038/s41477-024-01824-7

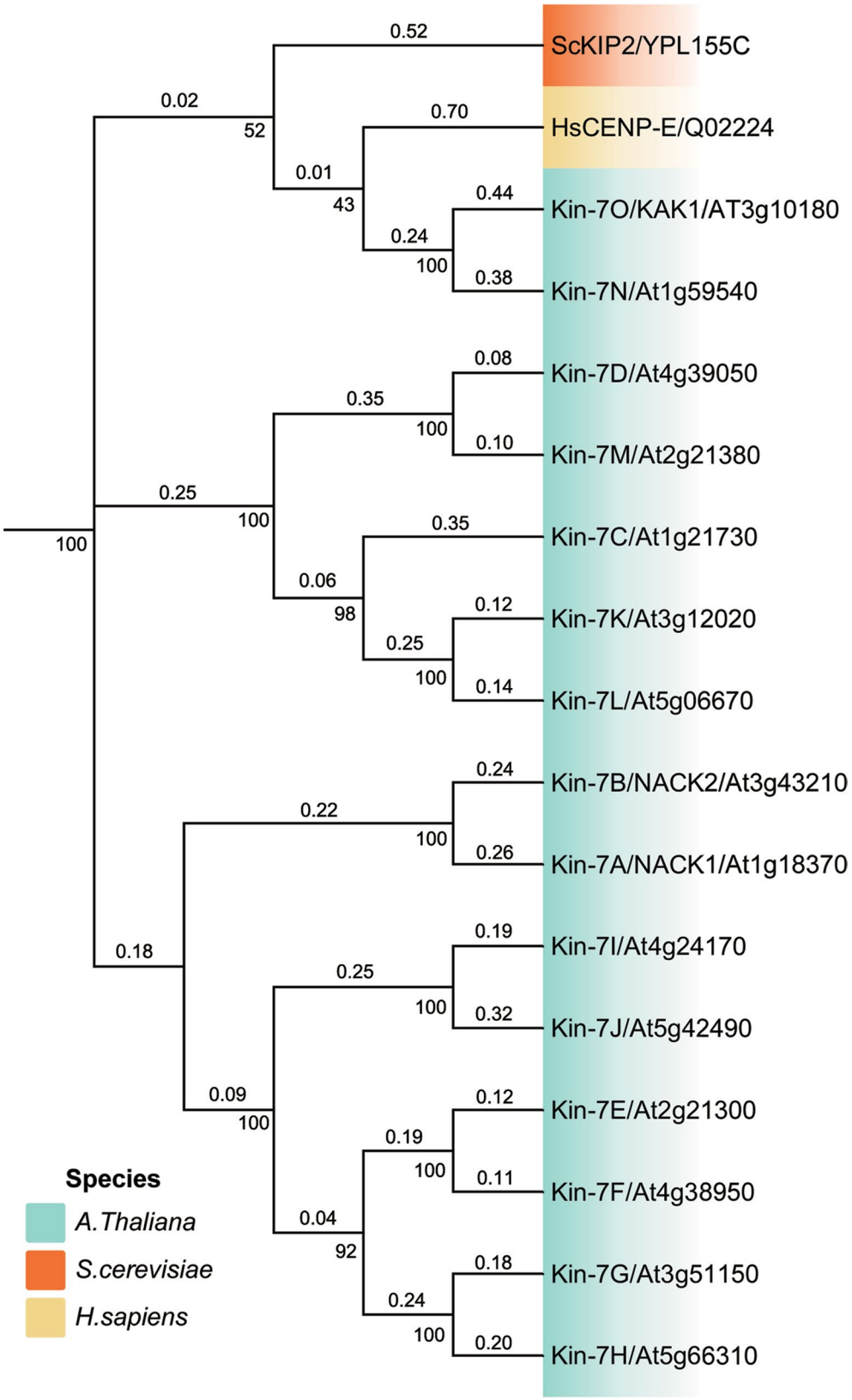

Extended Data Fig. 1 | KAK1 belongs to the kinesin-7 group. The phylogenetic tree shows the evolutionary relationship of the KAK1 protein from the plant species *A. thaliana* to other members of the kinesin-7 subfamily, including CENP-E from *H. sapiens* and KIP2 from *S. cerevisiae*. Amino acid sequences are aligned using the MUSCLE method. The tree is constructed using the neighbor-joining method within MEGA software, with gaps automatically removed using the complete-deletion option. The estimated evolutionary distances are indicated by the numbers above each branch, representing amino acid substitutions per site. The reliability of each branch is shown by the score next to each node, with the highest value being 100.

https://doi.org/10.1038/s41477-024-01824-7

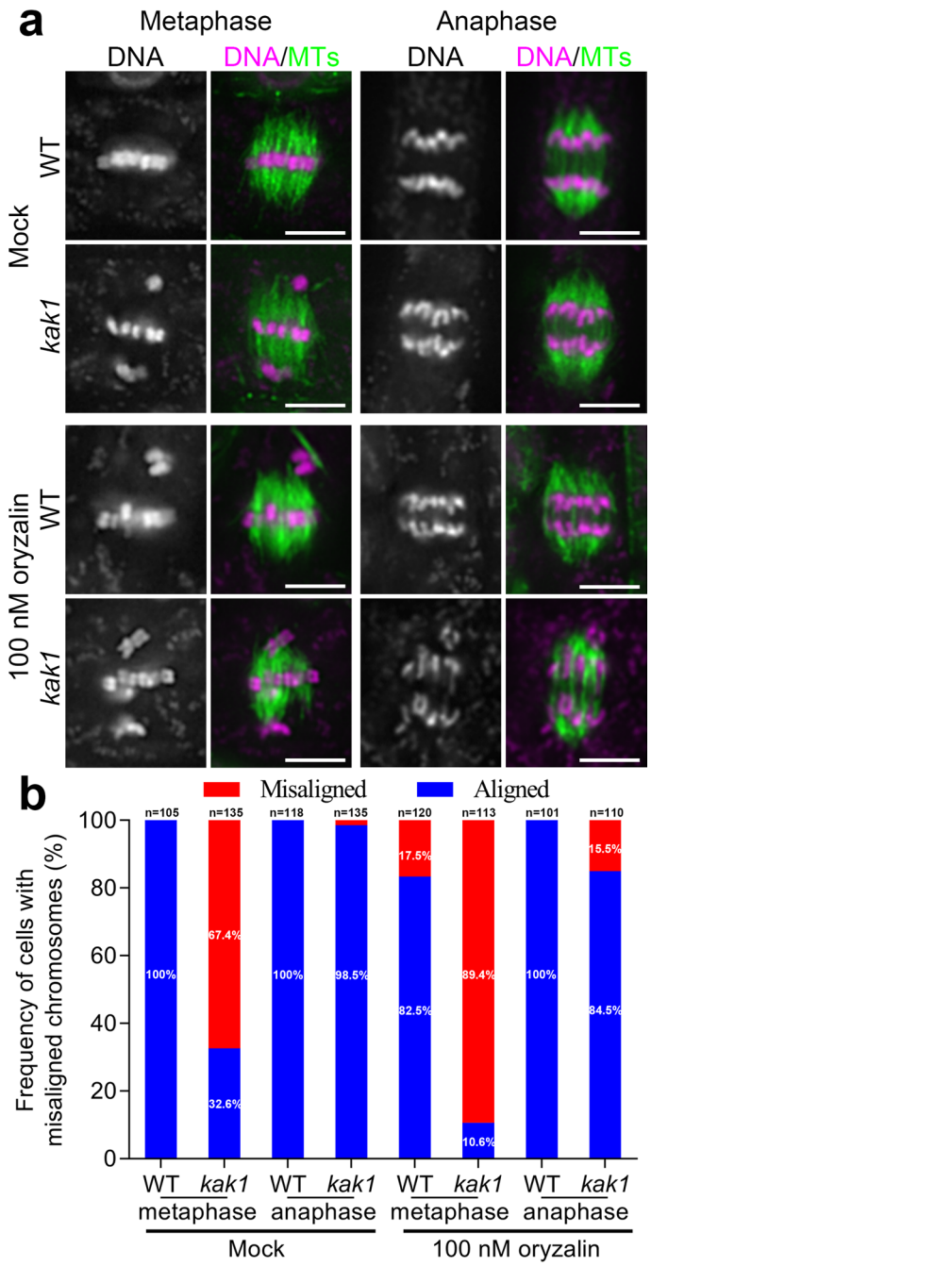

Extended Data Fig. 2 | Defective chromosome congression in the *kak1* mutant. a, Chromosomes congression and segregation in WT and *kak1* plants with or without oryzalin treatment. The fluorescent signals are detected by immunofluorescence, with MTs detected by the anti-tubulin antibody shown in green, and DNA detected by DAPI shown in magenta. Scale bars, 5 μm. **b**, Quantitative assessment of cells exhibiting misaligned chromosomes at metaphase and anaphase.

https://doi.org/10.1038/s41477-024-01824-7

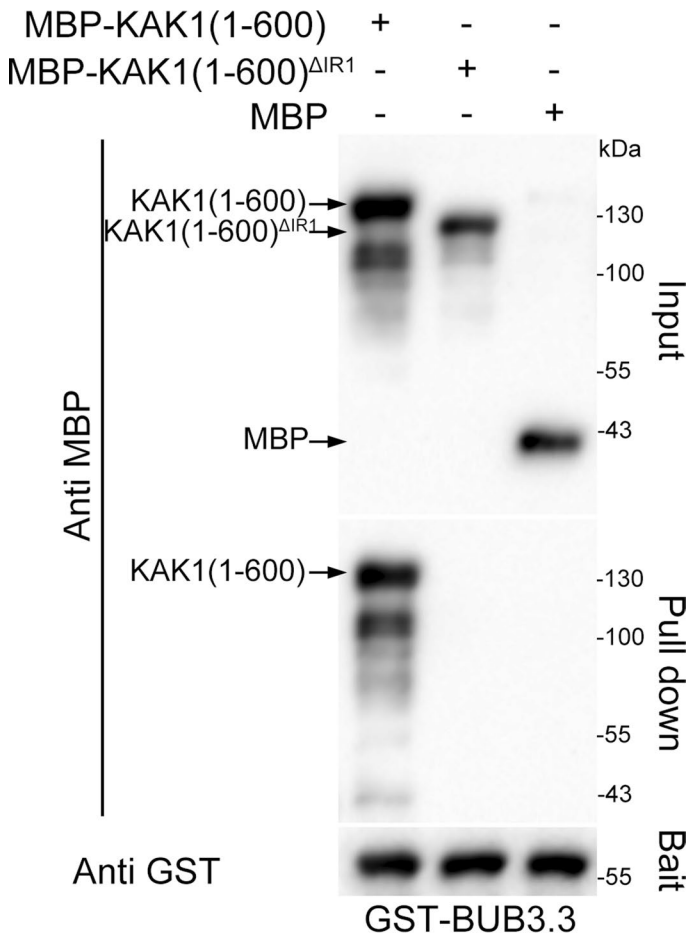

Extended Data Fig. 3 | Pull-down assays of recombinant MBP fusions of KAK1 variants with GST- BUB3.3 immobilized beads. The additional bands in the KAK1(1-600) sample line likely correspond to degradation products of the KAK1 N-terminal fragment during the co-purification process. The experiment was repeated three times with similar results.

https://doi.org/10.1038/s41477-024-01824-7

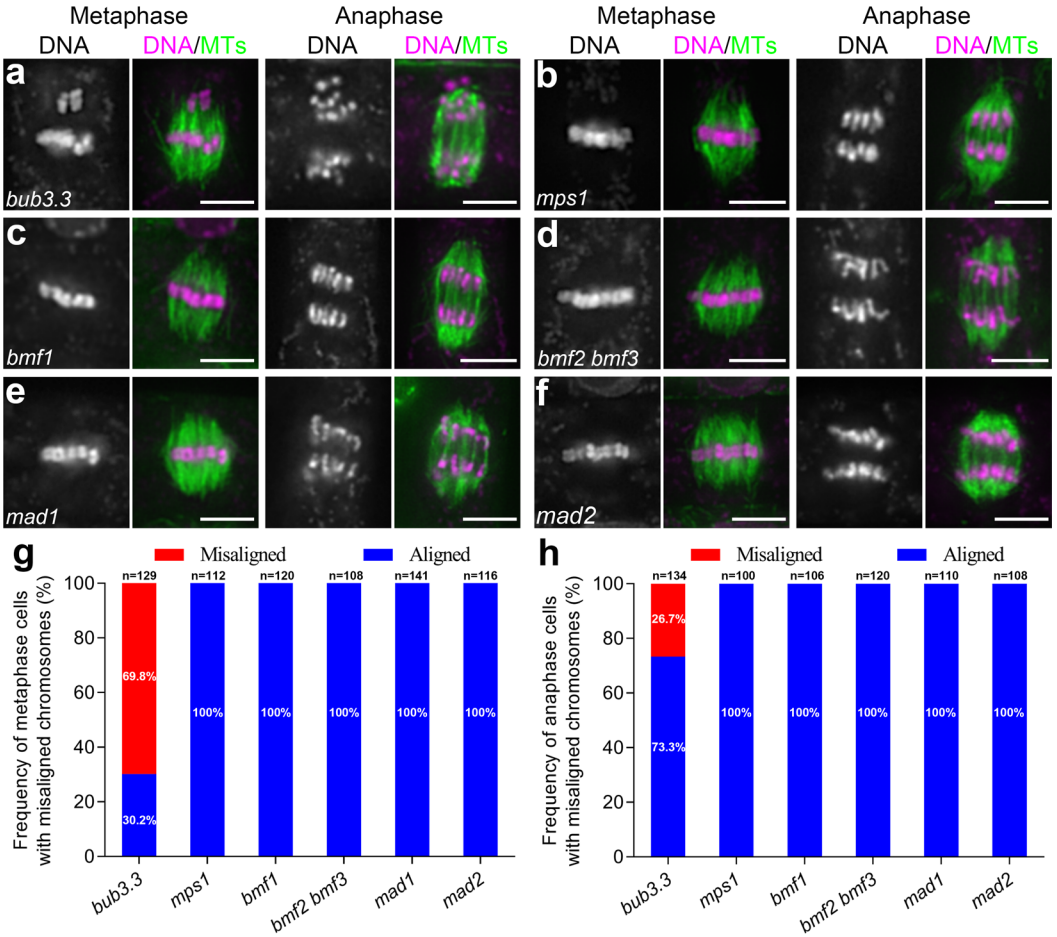

Extended Data Fig. 4 | Impact of SAC mutants on chromosome congression. **a-f**, Representative immunofluorescence images of mitotic cells from different SAC mutant backgrounds, including *bub3.3* (**a**), *mps1* (**b**), *bmf1* (**c**), *bmf2 bmf3* (**d**), *mad1* (**e**), and *mad2* (**f**). The MTs are visualized in green using an anti-tubulin antibody, and DNA is stained with DAPI (magenta). Scale bars, 5 μm. **g-h**, Quantitative assessment of cells exhibiting misaligned chromosomes at metaphase (**g**) and anaphase (**h**) in different SAC mutant backgrounds.

https://doi.org/10.1038/s41477-024-01824-7

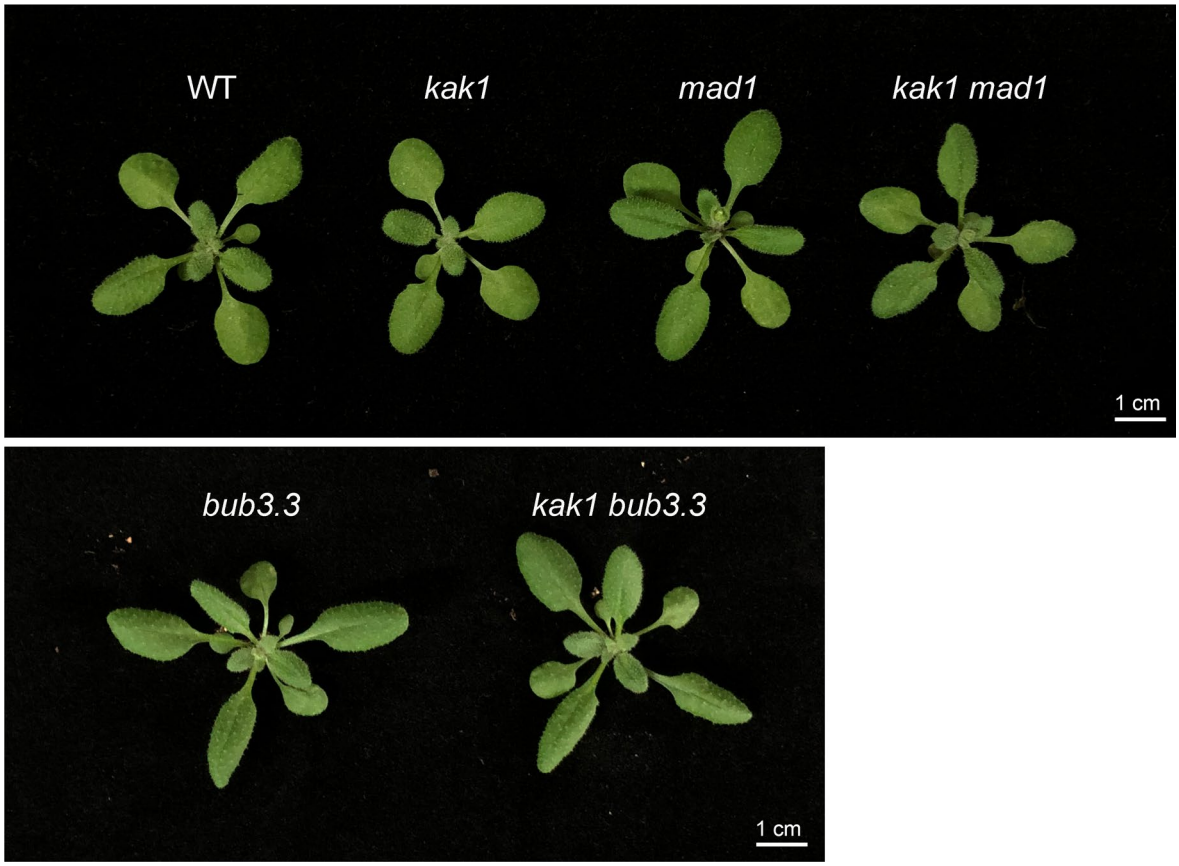

Extended Data Fig. 5 | Loss of *KAK1* in *mad1* and *bub3.3* mutants does not affect plant growth. Representative image of growth phenotypes of 3-week-old WT, *kak1*, *mad1*, *kak1 mad1*, *bub3.3*, and *kak1 bub3.3* plants. Scale bars, 1 cm.

https://doi.org/10.1038/s41477-024-01824-7

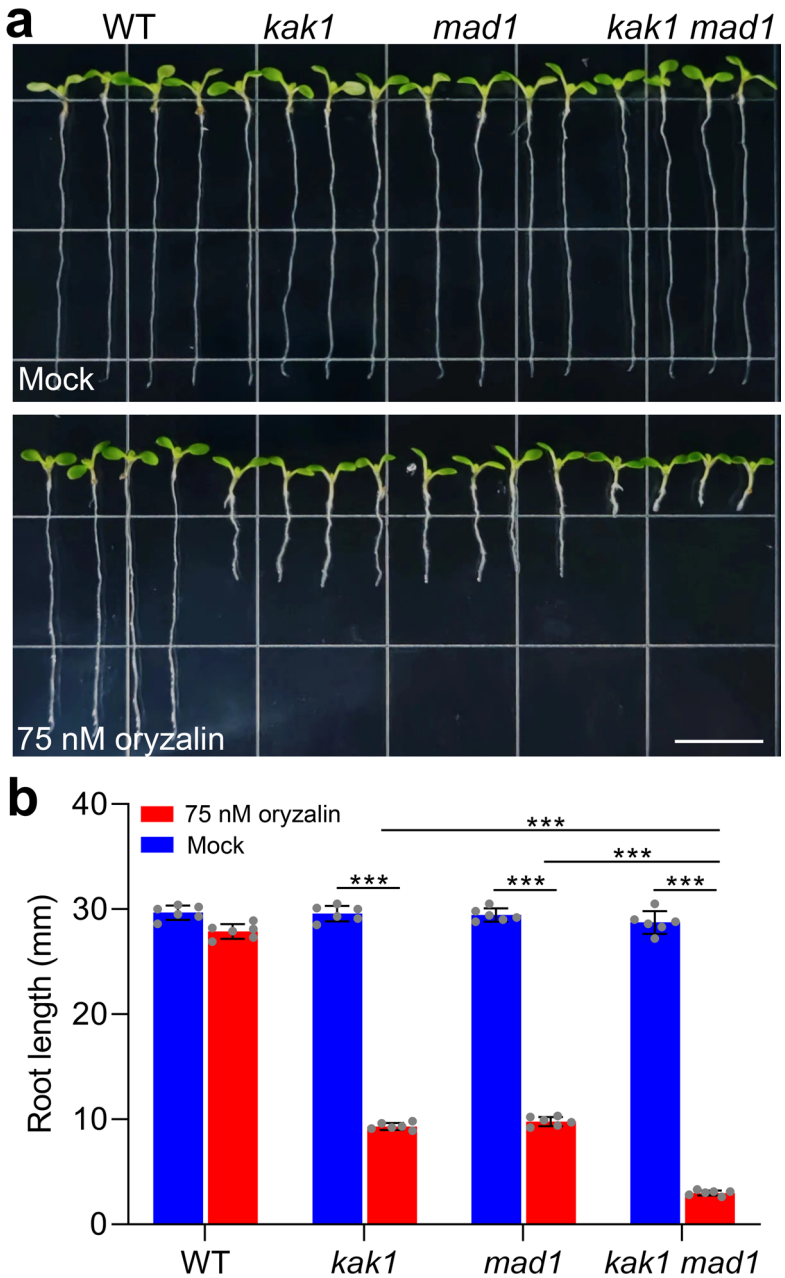

Extended Data Fig. 6 | The *kak1 mad1* double mutant exhibits increased sensitivity to oryzalin treatment. a, Representative images of 10-day-old seedlings of the WT, *kak1*, *mad1*, and *kak1 mad1* genotypes, grown either with or without 75 nM oryzalin. Scale bars, 1 cm. **b**, Quantification of root lengths in the seedlings with and without oryzalin treatment. Graph bars represent means ± SD of six seedlings per genotype. The statistical significance (***$P < 10^{-6}$) was determined by one-way ANOVA followed by Tukey test. The experiment was repeated three times with similar results.

https://doi.org/10.1038/s41477-024-01824-7

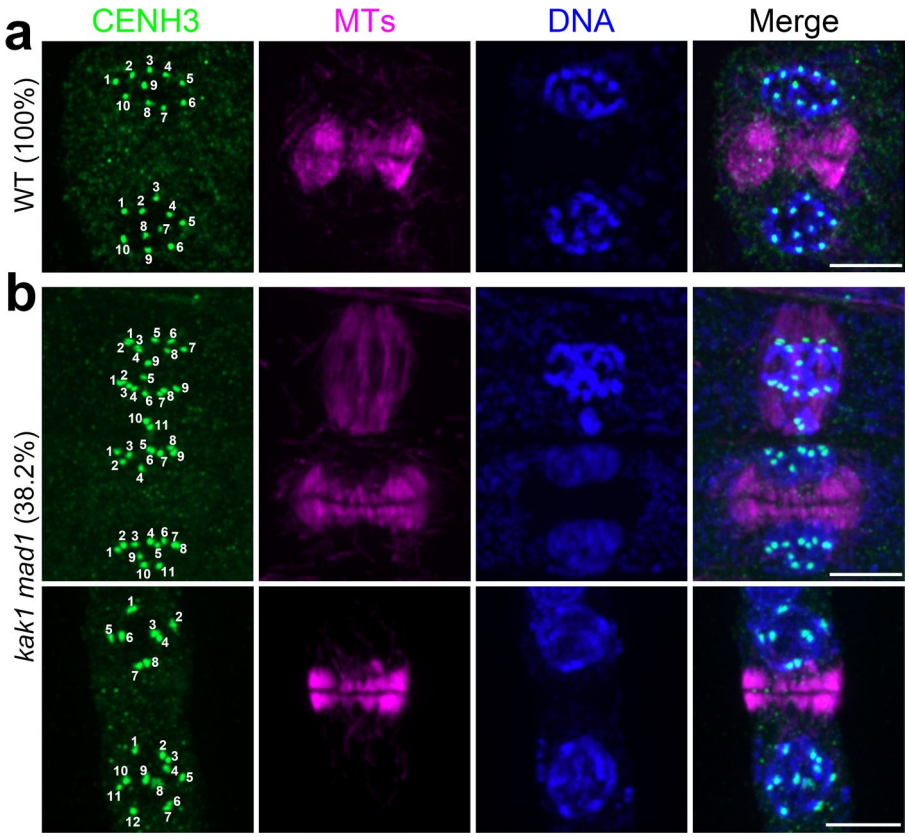

Extended Data Fig. 7 | The *kak1 mad1* double mutant generates aneuploid daughter cells. a, Representative immunofluorescence images of WT cells (n = 52) at the end of mitosis, where the forming daughter cells consistently exhibit 10 kinetochore signals, as detected by the anti-CENH3 antibody (green). The MTs (magenta) and DNA (blue) are also visualized. **b**, Representative immunofluorescence images of *kak1 mad1* mutant cells (n = 55) displaying aberrant chromosome segregation patterns. In the double mutant cells, the daughter cell pairs exhibit an unequal distribution of kinetochore signals, with pairs having 9 + 11 or 8 + 12 CENH3 signals. The immunofluorescence images are obtained through confocal-based z-stack projections of cells undergoing cytokinesis, allowing the visualization of all kinetochore signals in the forming daughter cells. Scale bars, 5 µm.

https://doi.org/10.1038/s41477-024-01824-7

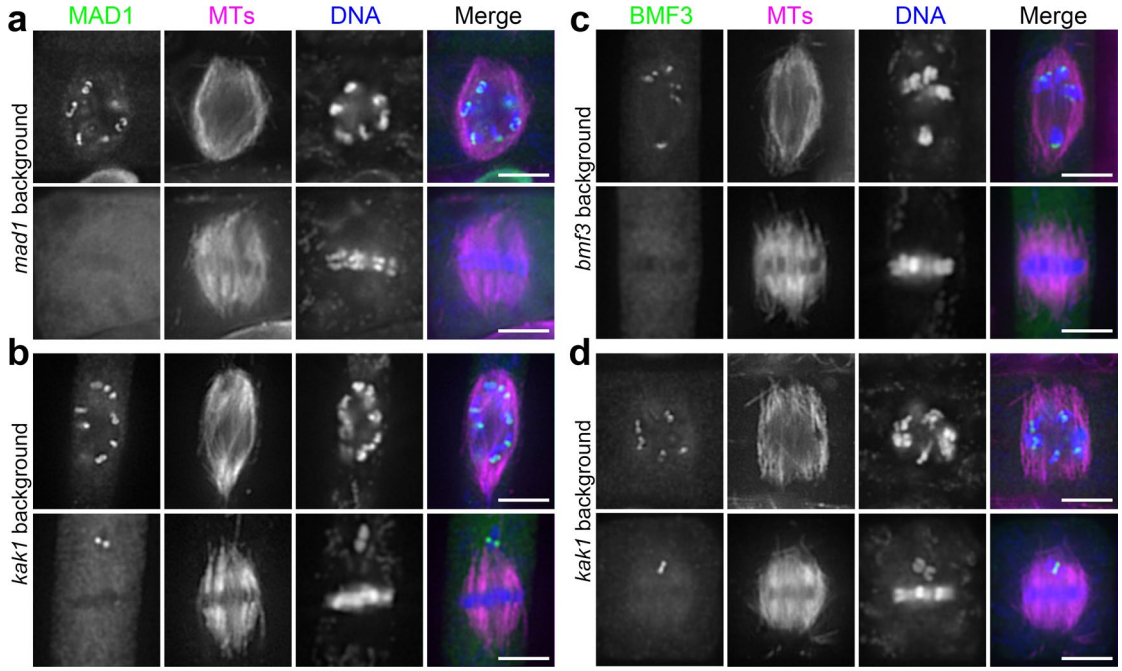

Extended Data Fig. 8 | KAK1 is not essential for kinetochore localization of core SAC proteins. a-b, GFP-MAD1 is detected at kinetochores upon expression in *mad1* mutant (**a**) and *kak1* mutant (**b**) backgrounds in representative cells at prophase (top row) and metaphase (bottom row). **c-d**, BMF3-GFP is detected at kinetochores upon expression in *bmf3* mutant (**c**) and *kak1* (**d**) mutant backgrounds. The fluorescent signals are detected by immunofluorescence and merged images have GFP-tagged proteins detected by anti-GFP shown in green, MTs detected by anti-tubulin shown in magenta, and DNA detected by DAPI shown in blue. Micrographs are representative of more than 60 cells from three independent lines with similar results. Scale bars, 5 μm.

nature portfolio

Corresponding author(s): Xingguang Deng

Last updated by author(s): Sep 4, 2024

Reporting Summary

Nature Portfolio wishes to improve the reproducibility of the work that we publish. This form provides structure for consistency and transparency in reporting. For further information on Nature Portfolio policies, see our Editorial Policies and the Editorial Policy Checklist.

Statistics

For all statistical analyses, confirm that the following items are present in the figure legend, table legend, main text, or Methods section.

n/a	Confirmed	
☐	☒	The exact sample size (*n*) for each experimental group/condition, given as a discrete number and unit of measurement
☐	☒	A statement on whether measurements were taken from distinct samples or whether the same sample was measured repeatedly
☐	☒	The statistical test(s) used AND whether they are one- or two-sided *Only common tests should be described solely by name; describe more complex techniques in the Methods section.*
☒	☐	A description of all covariates tested
☒	☐	A description of any assumptions or corrections, such as tests of normality and adjustment for multiple comparisons
☐	☒	A full description of the statistical parameters including central tendency (e.g. means) or other basic estimates (e.g. regression coefficient) AND variation (e.g. standard deviation) or associated estimates of uncertainty (e.g. confidence intervals)
☐	☒	For null hypothesis testing, the test statistic (e.g. *F*, *t*, *r*) with confidence intervals, effect sizes, degrees of freedom and *P* value noted *Give P values as exact values whenever suitable.*
☒	☐	For Bayesian analysis, information on the choice of priors and Markov chain Monte Carlo settings
☒	☐	For hierarchical and complex designs, identification of the appropriate level for tests and full reporting of outcomes
☒	☐	Estimates of effect sizes (e.g. Cohen's *d*, Pearson's *r*), indicating how they were calculated

Our web collection on statistics for biologists contains articles on many of the points above.

Software and code

Policy information about availability of computer code

Data collection	Immunofluorescence staining micrographs were captured using the PCO camware 4.17.1 (PCO Imaging) equipped with a Nikon Eclipse 600 microscope. Live cell imaging data were captured by the Zen 2 software (Carl Zeiss) equipped with a Zeiss LSM880 spinning-disk confocal microscope.
Data analysis	Statistical analyses (mean, standard deviation, and ANOVA test) were conducted using Graphpad Prism 9.0.0. Image analysis and assembly were conducted using Fiji ImageJ-win32 and Photoshop CS6 (Adobe).

For manuscripts utilizing custom algorithms or software that are central to the research but not yet described in published literature, software must be made available to editors and reviewers. We strongly encourage code deposition in a community repository (e.g. GitHub). See the Nature Portfolio guidelines for submitting code & software for further information.

Data

Policy information about availability of data

All manuscripts must include a data availability statement. This statement should provide the following information, where applicable:

- Accession codes, unique identifiers, or web links for publicly available datasets
- A description of any restrictions on data availability
- For clinical datasets or third party data, please ensure that the statement adheres to our policy

All data of this study are available in the main text or the supplementary information. Source data are provided with this paper.

Research involving human participants, their data, or biological material

Policy information about studies with human participants or human data. See also policy information about sex, gender (identity/presentation), and sexual orientation and race, ethnicity and racism.

Reporting on sex and gender	Not applicable
Reporting on race, ethnicity, or other socially relevant groupings	Not applicable
Population characteristics	Not applicable
Recruitment	Not applicable
Ethics oversight	Not applicable

Note that full information on the approval of the study protocol must also be provided in the manuscript.

Field-specific reporting

Please select the one below that is the best fit for your research. If you are not sure, read the appropriate sections before making your selection.

☒ Life sciences ☐ Behavioural & social sciences ☐ Ecological, evolutionary & environmental sciences

For a reference copy of the document with all sections, see nature.com/documents/nr-reporting-summary-flat.pdf

Life sciences study design

All studies must disclose on these points even when the disclosure is negative.

Sample size	No statistical measures were used to predetermine sample size. The experimental sample sizes were estimated based on our past experience in performing similar experiments or published papers, which were described in relevant figure legends and supplementary information.
Data exclusions	No data were excluded from our analyses.
Replication	All experiments were repeated at least three times with similar results, the numbers of independent lines or replicates were indicated in relevant figures or figure legends.
Randomization	For oryzalin treatment experiments, plants of the different genotypes were randomly selected to measure root length. For immunostaing experiments, cells at different mitotic stages were collected randomly.
Blinding	For oryzalin sensitive experiments, blinding is not applicable in data collection because of the obvious differences between control and mutant samples. For cell biological experiments, blinding was not required because the results of such measurements are directly obtained through microscope, and thus are not affected by sample identities.

Reporting for specific materials, systems and methods

We require information from authors about some types of materials, experimental systems and methods used in many studies. Here, indicate whether each material, system or method listed is relevant to your study. If you are not sure if a list item applies to your research, read the appropriate section before selecting a response.

Materials & experimental systems

n/a	Involved in the study
☐	☒ Antibodies
☒	☐ Eukaryotic cell lines
☒	☐ Palaeontology and archaeology
☒	☐ Animals and other organisms
☒	☐ Clinical data
☒	☐ Dual use research of concern
☐	☒ Plants

Methods

n/a	Involved in the study
☒	☐ ChIP-seq
☒	☐ Flow cytometry
☒	☐ MRI-based neuroimaging

Antibodies

Antibodies used

Primary antibodies used in this study were as follows:
1. GFP recombinant rabbit monoclonal antibody (1:500) (Thermo Fisher Scientific, Catalog #G10362).
2. DM1A mouse anti-α-tubulin monoclonal antibody (1:1,000) (Abcam, Catalog #ab7291).
3. 9A3 mouse anti-FLAG monoclonal antibody (1:1,000, Cell Signaling Technology, Catalog #8146).
4. Rabbit anti-CENH3 polyclonal antibody (1:500) (PhytoAB, Catalog #PHY7449A).
5. Mouse anti-MBP monoclonal antibody (1:10,000) (GenScript, Catalog #A00190).
6. Mouse anti-GST monoclonal antibody (1:10,000) (GenScript, Catalog #A00865).

Secondly antibodies used in this study were as follows:
7. Alexa fluor 488-conjugated goat anti-rabbit IgG (1:1,000) (Thermo Fisher Scientific, Catalog #A32731).
8. Alexa fluor 555-conjugated goat anti-mouse IgG (1:1,000) (Thermo Fisher Scientific, Catalog #A32727).
9. HRP-conjugated goat anti-mouse IgG (1:10,000) (Thermo Fisher Scientific, Catalog #31430).

Validation

All antibodies used in this study were commercial antibodies validated by the manufacturers as indicated on their web sites:
1. GFP recombinant rabbit monoclonal antibody (https://www.thermofisher.com/antibody/product/GFP-Antibody-Recombinant-Monoclonal/G10362).
2. DM1A mouse anti-α-tubulin monoclonal antibody (https://www.abcam.com/products/primary-antibodies/alpha-tubulin-antibody-dm1a-loading-control-ab7291.html).
3. 9A3 mouse anti-FLAG monoclonal antibody (https://www.cellsignal.com/products/primary-antibodies/dykddddk-tag-9a3-mouse-mab-binds-to-same-epitope-as-sigma-aldrich-anti-flag-m2-antibody/8146).
4. Rabbit anti-CENH3 polyclonal antibody (https://www.phytoab.com/cenh3.-antibody).
5. Mouse anti-MBP monoclonal antibody (https://www.genscript.com.cn/antibody/A00190-MBP_tag_Antibody_mAb_Mouse.html)
6. Mouse anti-GST monoclonal antibody (https://www.genscript.com.cn/antibody/A00865-THE_GST_Antibody_mAb_Mouse.html)
7. Alexa fluor 488-conjugated goat anti-rabbit IgG (https://www.thermofisher.com/antibody/product/Goat-anti-Rabbit-IgG-H-L-Highly-Cross-Adsorbed-Secondary-Antibody-Polyclonal/A32731)
8. Alexa fluor 555-conjugated goat anti-mouse IgG (https://www.thermofisher.com/antibody/product/Goat-anti-Mouse-IgG-H-L-Highly-Cross-Adsorbed-Secondary-Antibody-Polyclonal/A32727)
9. HRP-conjugated goat anti-mouse IgG (https://www.thermofisher.com/antibody/product/Goat-anti-Mouse-IgG-H-L-Secondary-Antibody-Polyclonal/31430)

Dual use research of concern

Policy information about dual use research of concern

Hazards

Could the accidental, deliberate or reckless misuse of agents or technologies generated in the work, or the application of information presented in the manuscript, pose a threat to:

No	Yes	
☒	☐	Public health
☒	☐	National security
☒	☐	Crops and/or livestock
☒	☐	Ecosystems
☒	☐	Any other significant area

Experiments of concern

Does the work involve any of these experiments of concern:

No	Yes	
☒	☐	Demonstrate how to render a vaccine ineffective
☒	☐	Confer resistance to therapeutically useful antibiotics or antiviral agents
☒	☐	Enhance the virulence of a pathogen or render a nonpathogen virulent
☒	☐	Increase transmissibility of a pathogen
☒	☐	Alter the host range of a pathogen
☒	☐	Enable evasion of diagnostic/detection modalities
☒	☐	Enable the weaponization of a biological agent or toxin
☒	☐	Any other potentially harmful combination of experiments and agents

Plants

Seed stocks	kak1 mutant: SALK_115677; bub3.3 mutant: SALK_022904; bmf1 mutant: SALK_122554; bmf2 mutant: SAIL_303_E05; bmf3 mutant: SALK_032111; mad1 mutant: SALK_073889; mps1 mutant: GABI_663H07; mad2 mutant: SAIL_191_G06
Novel plant genotypes	None
Authentication	None